Mitochondrial dynamics in the presence of neurodegenerative disease

Mary P. Nivison

A dissertation
submitted in partial fulfillment of the
requirements for the degree of

Doctor of Philosophy

University of Washington
2014

Reading Committee:
Philip J. Horner, chair
John I. Clark
Jean S. Campbell
Thomas N. Wight

Program Authorized to Offer Degree:
Pathology

University of Washington

Abstract

Mitochodrial dynamics in the presence of neurodegenerative disease

Mary P. Nivison

Chair of Supervisory Committee
Professor Philip J. Horner
Department of Neurological Surgery

Mitochondrial dysfunction is an early event in many neurodegenerative diseases, with impaired bioenergetics and migration acting as neurodegenerative triggers. Mitochondrial disruption in the form of reduced bioenergetic capacity, increased oxidative stress and reduced resistance to stress is observed in several disease models. Mitochondria are essential for cellular function due to their role in ATP production, metabolic regulation, cell cycling, signaling pathways, and development. Neurons are responsible for buffering calcium fluxes during synaptic transmission while providing the energy for vesicle release and recycling, maintenance of membrane potential, and axonal and dendritic transport. Maintaining healthy mitochondria is crucial to meet the bioenergetic demands of a neuron and is achieved by maintaining a careful balance between mitochondrial biogenesis, transport, dynamics and mitophagy. In glaucoma, increased intraocular pressure is a stressor for ganglion cells and is implicated in dysfunction of the mitochondrial fusion proteins, Mitofusin 1 and Mitofusin 2, that regulate mitochondrial dynamics and transport. Here we propose that post-translational modifications of mitofusins disrupt mitochondria dynamics and transport. We found impaired mitochondrial dynamics and transport result in the accumulation of Mitofusin 2 in the somas of the retinal ganglion cells, intervening in the dissemination of energy throughout the axons, resulting in the eventual death

of the neurons. Based on our findings, we propose a mechanism by which mitochondrial dysfunction is triggered in glaucoma via intraocular pressure through the inactivation of kinases.

Table of Contents

List of Figures

Acknowledgements

I would like to thank my two main mentors, Philip Horner and Jean Campbell. Phil took me into his lab and encouraged me through all the ups and downs inherent in scientific research. Over the years, both Phil and Jean continued to believe in me when I didn't believe in myself, and prodded me to become the best scientist I could be. To all my committee members for having stuck with me through everything, and helped me at every turn with their own expertise and time, as well as placing their labs at my disposal, I thank you. I would like to thank my collaborators Jason Bielas, David Calkins, and their labs for the assistance in performing experiments and teaching me techniques. Thanks to Heidi Back, my assistant, for her help with both experiments and technology problems. I would like to thank the Pathology Department, especially Dan Bowen-Pope, Steve Berard, and Kathy Hobson for all their support and help navigating the grad school waters, and Nelson Fausto, who took me into his lab and taught me high scientific standards. To my former colleagues in other labs, Claudia Mitchell, Melissa Odell Johnson, and Renay Bauer, I appreciate your continued teachings all the way through this endeavor. I would like to thank all my former class members, Roland, Marc, Jenny, Jenn, Myra, Leslie, and especially Ingrid, who helped me through both scientific obstacles and difficult personal times.

Additional thanks to my family and friends for support- emotional, physical, financial or otherwise- for believing in me, and even being inspired by me.

It truly takes a village…

Dedication

To my family, both blood and chosen

Part I: Introduction

Glaucoma

Glaucoma is an eye disorder in which the optic nerve becomes damaged, permanently impairing vision and progressing to complete blindness if untreated. It has been nicknamed the "silent thief of sight" because the loss of vision normally occurs gradually over a long period of time, and is often only recognized when the disease is quite advanced and vision is already compromised. Once lost, the damaged visual field cannot be recovered.

Historically, glaucoma has been thought of as a disease caused by excessive pressure in the posterior chamber of the eye. More recently, it has been seen as a neurodegenerative disorder characterized by progressive deterioration of the optic nerve axons and slow decline and death of retinal ganglion cells (RGCs) seen in the axonal degeneration and eventual RGC soma loss in the retina (Calkins and Horner, 2012). As glaucoma progresses, RGC axons are compromised in many ways, including a decrease in ATP production and disruption of mitochondrial transport (Baltan et al., 2010; Knott et al., 2008). In our lab, we have previously shown that the axons of DBA mice are more susceptible to metabolic challenges, with their ability to recover severely compromised (Baltan et al., 2010). Our lab also showed that mitochondria are short and punctate in healthy RGCs, while in the diseased cells they are elongated or fused and tend to cluster more tightly around the nucleus with fewer seen in their axons (Uo et al., 2009).

While age and intraocular pressure (IOP) elevation are the main risk factors in glaucoma, all age groups and people with normal IOP can be affected, suggesting that other events play a role in the loss of RGC viability (Bosco et al., 2011; Libby et al., 2005; Whitmore et al., 2005).

There are two main categories of glaucoma, open angle and closed angle. Closed angle glaucoma often appears suddenly and can be painful; visual loss progresses quickly, but the discomfort often leads patients to seek medical attention before permanent damage occurs. Open angle, which comprises 70 percent to 80 percent of the cases, is generally accepted to occur due to an imbalance in the production and drainage of aqueous humor. The trabecular meshwork normally drains the fluid from inside the eye, but cannot because it becomes clogged or inflamed and functions improperly, and can cause increased IOP (Ferrer, 2006). Open angle glaucoma tends to progress at a slower rate and may go unnoticed until visual loss has already begun.

There is continuing, ongoing investigation into better understanding of the mechanisms underlying the RGC loss occurring in glaucoma (Knott et al., 2008). To tease out the role which pressure alone plays on RGCs, the Calkins lab has isolated RGCs from post-natal rat retinas, cultured them and subjected them to pressure that recapitulates the levels seen in disease. It was determined that the cells subjected to pressure had a decreased density as pressure was maintained over longer time periods (up to 48 hours). Also, the pressurized cells had an increased rate of TUNEL staining, reflecting an increased amount of apoptosis occurring in the cells with elevated pressure. These findings indicate that sustained pressure does indeed play a role in RGC loss in high IOP glaucoma (Sappington et al., 2006).

Axonal degeneration of the optic nerve is an important hallmark for models of glaucoma involving increased IOP (McKinnon et al., 2009; Morrison, 2005; Morrison et al., 1997). Recently, an acute model of glaucoma was developed which causes moderate glaucomatous changes in response to sustained elevated IOP. In this paradigm, small microbeads are injected into the anterior chamber of the rodent eye. Microbead injection is limited to one eye, with the other eye receiving an equivalent volume of saline, acting as an internal control for the surgical procedure. These beads create blockage of the trabecular meshwork, which creates a disruption of the normal flow of the aqueous humor and causes pressure to build up within the posterior chamber of the eye, eliciting reliable elevations in IOP of about 30% which persists for slightly more than 3 weeks. This model, called the microbead occlusion model, causes a sustained IOP for several weeks (Sappington RM, 2006).

By quantifying mean axon density and number of axons, the effect of pressure on the RGCs was found to include a modest but measurable thinning of the axon population in the optic nerve after 4 to 5 weeks. This thinning is concurrent with signs of the typical hallmarks of glaucomatous pathology (gliosis, degenerating profiles, disorganization) and demonstrates clear axonal disorder, reduction in axon packing, and axonal distension (Sappington RM, 2006).

This tool allows for assessment of pressure effects without the confounding genetic effects that might occur during development. By subjecting an otherwise normally developing population of cells to acute glaucoma, it is possible to focus on non-genetic causes of susceptibility to pressure.

Mouse model

For the majority of the experiments produced for this body of work, the DBA2/J mouse model of glaucoma was utilized. A vital tool for studying glaucoma, the DBA/2J (DBA) mice are a well-established mouse model of glaucoma (John et al., 1998; Libby et al., 2005; Rangarajan et al., 2011). These mice have spontaneously developed two ocular phenotypes, iris stromal atrophy (ISA) and iris pigment dispersion (IPD) (Chang et al., 1999; John et al., 1998), that are caused by mutations in the *Tyrp1* and *Gpnmb* genes, respectively. *Tyrp1* (tyrosinase-related protein 1) has two missense mutations that cause amino acid substitutions and alter protein folding, to yield a non-functional protein product, causing ISA (Anderson et al., 2002). The gene responsible for the IPD phenotype, *Gpnmb* (glycoprotein transmembrane nmb), has a point mutation that creates a premature stop codon which yields a truncated protein on translation (Anderson et al., 2002).

As a result of these two mutations, DBA mice develop elevated IOP and glaucoma with age, in a similar fashion as humans. Due to similarities to closed angle glaucoma, these mice are now widely used as a surrogate model for human glaucoma (Howell et al., 2007). In the DBA mice, there is decreased axon transport at 6-9 months (Buckingham et al., 2008; Soto et al., 2008), increased oxidative stress (Lambert W, 2008; Lambert WS, 2006), gliosis and microgliosis (Bosco et al., 2008; Inman and Horner, 2007), mitochondrial clumping (Horner lab unpublished data), neuronal shrinkage, and genetic downregulation of RGC specific genes (Buckingham et al., 2008; Soto et al., 2008).

The control mouse formerly used for the DBA mouse was the C57BL/6 (B6), which was not an ideal model due to strain-related genetic variation. Recently, another mouse was designed as close genetic match which has had the wild-type *Gpnmb* gene reinserted. This mouse, the DBA/2J^{Gpnmb+} (D2G), carries only one of the two mutations, the *Tyrp1*, and does not develop glaucoma, making them an ideal control animal for both disease and aging studies (Anderson et al., 2008). Throughout these experiments, unless specifically designated as B6, the D2G mice were used as age-matched controls.

In the first few months (designated young or pre-disease), the DBA does not show outward manifestations of disease, including IOP elevation. This begins to change at five to six months, the early disease stage, when there is increasing IOP, decreasing optic nerve function, and metabolic deficit. In the late, chronic stage (designated aged or chronic), the optic nerve is

badly degenerated, many RGCs are dead or dying, the mice are functionally blind, and ATP production is severely curtailed (Baltan et al., 2010; Buckingham et al., 2008; Inman et al., 2013; Lambert W, 2008). Figure 1.1 shows a progression of the disease charted by intraocular pressure.

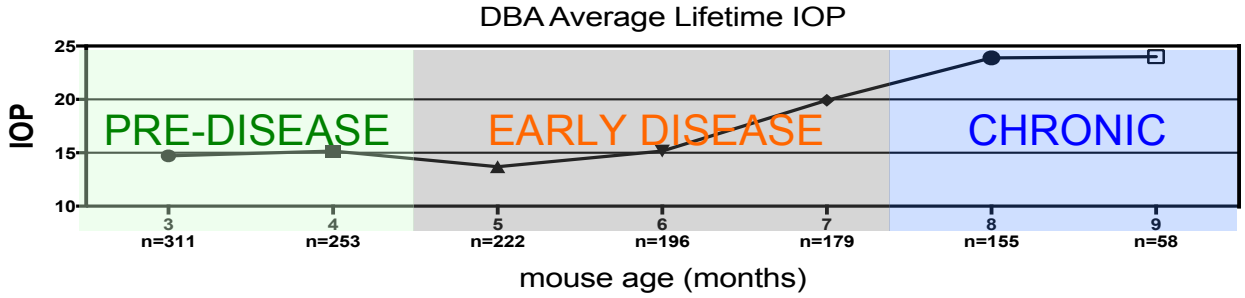

Figure 1.1. DBA average lifetime IOP versus disease progression

Age-matched animals were used in all experiments. Young animals were 3 months old; 6 month animals were 5-7 months; aged animals were 9-13 months.

Eye and structure

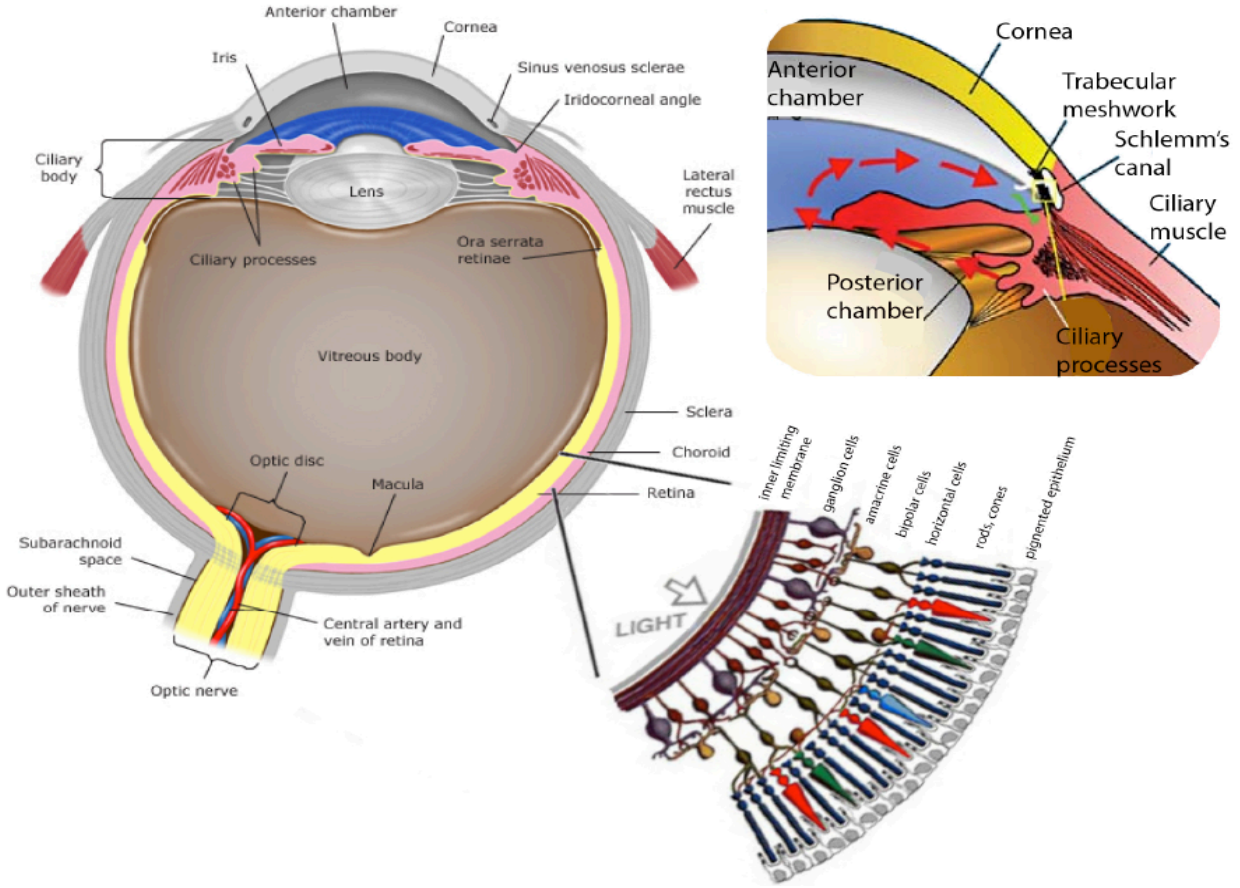

Figure 1.2 Diagram of the eye. Image on the left shows the main eye structures(30). Upper right image illustrates the angle, with the trabecular meshwork and Schlemm's canal (Ferrer, 2006). Lower right shows a breakdown by layer of the retina (webvision.med.utah.edu).

The eye is an organ that responds to light. Light enters the eye through the pupil and passes through the many layers of the retina to the photoreceptors, the rods and cones, at the outer nuclear layer. There the light is translated and the information is then relayed back up through the layers to the ganglion cells (RGCs) whose axons form the optic nerve. The optic nerve carries the information to the visual cortex in the brain.

In figure 1.2 above, a depiction of the eye is given, with the inset in the upper right showing a closer look at the angle. The arrows represent the flow of the aqueous humor, the fluid in the eye. In the DBA model of glaucoma, there is a breakdown of the pigment in the iris which collects at the trabecular meshwork. This results in the flow of fluid thru the Schlemm's canal becoming blocked, causing fluid buildup and a resultant increase of intraocular pressure.

Mitochondria

Mitochondria are dual-membrane organelles contained within cells. As recently as 10 years ago, it was believed that mitochondria acted solely to supply cells with energy. It is now known that mitochondria are dynamically motile and regularly remodel themselves via fission and fusion. Aside from supplying energy, they play a role in metabolism and its regulation, cell cycle, signaling pathways, and development (McBride H, 2006). They are also involved in neuronal functions (Detmer and Chan, 2007).

In neurons, mitochondria are responsible for energy production, Ca^{2++} regulation, maintenance of membrane potential, axonal and dendritic transport and the release and reuptake of neurotransmitters at synapes (Knott et al., 2008; McBride H, 2006). Mitochondria are also responsive to synaptic activity, clustering at the sites of dendritic spines with synaptic activity. Mitochondria play an important functional role in buffering calcium fluxes during synaptic transmission, while providing the energy for vesicle release and recycling (McBride H, 2006).

Healthy mitochondria actively undergo fusion and fission as part of normal cell physiology. They actively communicate with each other, in part to satisfy the changing energy needs of the cell. Ongoing research has made a number of likely links between mitochondrial fusion and fission disruption and bioenergetic failure. For instance, lack of fusion has been linked to decreased ATP production, while lack of fission interferes with normal cell death (Knott et al., 2008).

Mitochondrial disruption is an early event in neurodegeneration (Johri and Beal, 2012), with impaired bioenergetics and migration acting as neurodegenerative triggers (Knott et al., 2008). Axonal transport mechanisms are disrupted, interfering with organelle transport, including mitochondria. An inability for the mitochondria to freely move and remodel themselves may contribute to the axonal degeneration and progression of the disease. Mitochondria play many key functional roles in the cell. Therefore, the decrease of ATP production and disruption of mitochondrial transport can readily be viewed as a pivotal cause underlying disease (Baltan et al., 2010). Conversely, disease may interfere with the cellular infrastructure, disrupting mitochondria's ability to function in its many necessary locations throughout a cell. In either case, the ability for mitochondria to function properly and disease are incontrovertibly linked (Detmer and Chan, 2007).

Whether mitochondrial mutations are present at a higher rate in disease is only beginning to be explored. Current mutational studies are ongoing in several forms of cancer to determine what effect, if any, they might play in compromising cellular function (Abramov et al., 2010; Vermulst et al., 2007). Whether these mutations might play a role in altered mitochondrial behavior and health in the confines of glaucoma has not been previously considered.

The RGCs' axons comprise the optic nerve. Degeneration of the nerve is the cause of loss of sight. In glaucoma, axonal transport is disrupted. Whether this disruption is the cause of the disease or resultant from the disease is still being evaluated. The effects of this breakdown of transport on mitochondria are also still being explored. Manipulating the balance between fusion and fission proteins may improve recovery or delay axonal degeneration.

Mitofusins

Mitochondria undergo continual cycles of fusion and fission. There are some key proteins involved in mitochondrial dynamics: mitofusin (Mfn) 1 and Mfn2 are fusion proteins located on the outer mitochondrial membrane and are directly involved in mitochondrial fusion (Santel and Fuller, 2001). Optic atrophy 1 (OPA1) is an inner membrane fusion protein, located in the intermembrane space. Dynamin-related protein (Drp)1 is involved in mitochondrial fission, as are the less well-studied fission proteins endophilin B1 and MTP18 (Chan, 2006b; Cho et al., 2010).

Mitochondrial fusion in mammals is controlled by two mitofusins, Mfn1 and Mfn2, GTPases localized to the mitochondrial outer membrane (Mozdy AD, 2003; Santel and Fuller, 2001). The mitofusins are required for embryonic development (Chen et al., 2003) and vascular smooth muscle cell proliferation (Guo et al., 2007). Reduced mitochondrial fusion results in dysfunction, with mutations in Mfn2 responsible for most cases of Charcot-Marie-Tooth type 2A disease, an inherited peripheral neuropathy (Zuchner et al., 2004). Mfn1 and Mfn2 are essential to both organism development and mitochondrial health, consequently understanding their responses under stress is important (Chen et al., 2003). The effects of stress on the breakdown of mitochondrial transport also need to be explored (Kiryu-Seo et al., 2010; Misko et al., 2010).

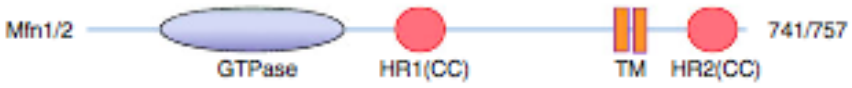

Figure 1.2. Schematic structure of Mfn 1 and Mfn2 domains. (Cho et al., 2010)

To elucidate the process by which mitofusins mediate mitochondrial fusion, other membrane trafficking systems, including endoplasmic reticulum–to–Golgi transport and synaptic vesicle fusion were studied. It was shown that mitochondria first tether to another nearby mitochondria, which allows fusion to occur (Koshiba et al., 2004). Mfn1 and Mfn2 form intertwining helical complexes between adjacent organelle membranes, linking them together. The HR2 domain initiates the tethering of two adjacent mitochondria (Cho et al., 2010).

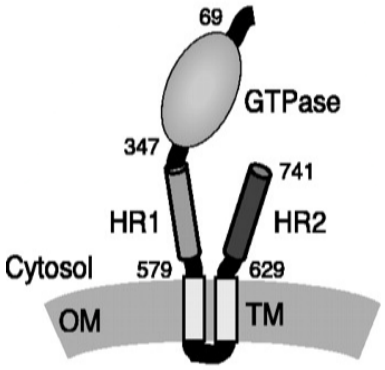

Figure 1.3. Structural basis of mitochondrial tethering by Mfn complexes (Koshiba et al., 2004).

These helices also anchor the mitochondria to the microtubule via kinesin for mitochondrial transport up and down the axons. Two key proteins, Miro and Milton, are involved in anchoring the mitochondria to the microtubules: Miro attaches to the mitochondrial membrane, while Milton is responsible for recruiting kinesin heavy chain to the mitochondrial surface. It was also determined there was another unknown protein in the protein complex located at the carboxy terminus of Milton which assisted in anchoring the complex to the mitochondria (Glater E, 2006). In continuing to explore the anchoring protein complex, it was determined Mfn2 was directly associated with Milton and Miro in dorsal root ganglion neurons,

thus supporting Mfn2's role in mitochondrial transport. It was further demonstrated that the mitofusins are necessary for transporting specifically mitochondria up and down axons, and that loss of Mfn2 is sufficient to produce severe transport deficits. Exogenous Mfn1 can rescue deficits caused by the loss of Mfn2. Finally, it was shown that depletion of Miro2 produces a mitochondrial transport deficit similar to loss of Mfn2 (Misko et al., 2010).

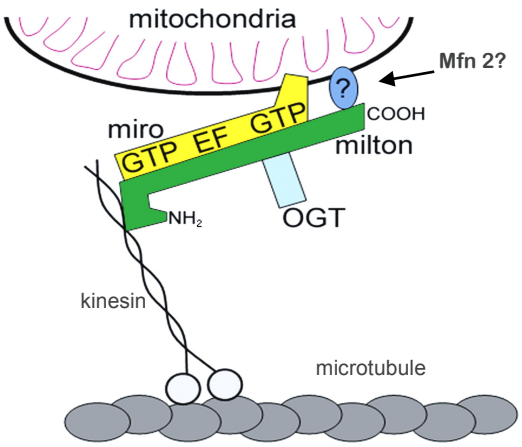

Figure 1.4. Depiction of the protein complex that mediates mitochondrial movement. (Glater E, 2006)

Opa1, genetically similar to the mitofusins, acts to link the inner membranes. Its role in fusion is still unclear, but knocking down Opa1 causes increased mitochondrial fragmentation and severe cristae malformations (Song et al., 2009). Opa 1 also acts to sequester pro-apoptotic cytochrome c molecules within the mitochondrial cristae spaces (Cipolat et al., 2006; Frezza et al., 2006). Genetic mutations in Opa1 cause autosomal dominant optic atrophy (DOA) (Davies et al., 2007; Hudson et al., 2008; Yu-Wai-Man et al., 2010a), one of the most common inherited optic neuropathies. Opa1 mutations are also linked to other clinical manifestations, most commonly including sensorineural deafness, ataxia, myopathy and progressive external ophthalmoplegia (Yu-Wai-Man et al., 2010b; Yu-Wai-Man et al., 2011). It was found that knocking down Opa1, the inner membrane fusion protein, does not alter mitochondrial axonal transport (Misko et al., 2010).

Dynamin-related protein (Drp)1 is involved in mitochondrial fission. Most of the Drp1 is found in the cytosol, with a small amount found in punctate spots on the mitochondrial membrane, often denoting future fission sites. Drp1 is recruited to the mitochondrial membrane for spiral formation and fission by another outer membrane protein, Fis1. Fis1 is a fission protein located on the outer membrane of the mitochondria which recruits the cytosolic Drp1 to encircle the mitochondria, and whose activity is dependent upon Drp1. Its involvement in attracting Drp1 to the membrane is unclear, but it is believed to act as a receptor for an unidentified protein ligand that causes Drp1 to collect at fission sites. However, Drp1 can still localize to the mitochondrial membrane in the absence of Fis1. Lack of Drp1 inhibits fission, resulting in elongated mitochondria (Chan, 2006b; Cho et al., 2010).

Examining changes in the fusion protein levels in both control (D2G) and diseased (DBA) animals at various ages and disease expression levels will generate a better understanding of the downstream effects of the presence or absence of the mitochondrial proteins. It will also indicate whether the disease causes damage to mitochondria or if the dying axons cause the mitochondrial dysfunction. Looking for preferential expression of the mitofusins in the different cellular compartments of the visual system will reveal whether such expression may contribute to the susceptibility created by the stressors induced by disease.

David Chan's group has studied mitochondria and Mfn2 quite extensively (Chan, 2006b; Chen et al., 2003; Koshiba et al., 2004; Song et al., 2009). In one study, it was determined that Mfn2 is preferentially expressed in the Purkinje cells of the cerebellum (Chen et al., 2007). Upon encountering these findings, as well as observing suggestive staining in the RGC layer of the retina, determining whether cell-specific expression of either mitofusin might be contributing to RGC vulnerability to high IOP and thus contributing to the degeneration of the RGC axons and transport disruption could be significant to exposing underlying mechanisms of the disease. With the more recent findings of the vital role played by Mfn2 in mitochondrial transport (Kiryu-Seo et al., 2010; Misko et al., 2010; Munemasa et al., 2010), the question of RGC specificity for Mfn1 or Mfn2 becomes even more crucial. By studying protein and RNA expression levels of both mitofusins through the course of glaucoma, a preferential expression of Mfn1 or Mfn2 in the retinal ganglion cells could shed light on what effect this might have on ganglion cell susceptibility to the disease.

Recently, findings from the Calkins lab demonstrated that RGCs *in vitro* suffer degenerative changes upon exposure to pressure levels which mimic high IOP. With the discovery of increased apoptosis in those cells as well, it clearly demonstrated that pressure has a negative impact on RGCs similar to that which is seen in glaucoma (Sappington et al., 2006). Considering this, it is likely that mitochondrial function in these cells is compromised as well. Knowing that mitofusin levels are altered in the retina in the presence of disease, further investigation into some of the variables that may be affected in association with mitochondria is warranted. Because the mitofusins are involved in fusion and transport, their role in the proper functionality of mitochondria needs to be clarified. A first step in this process can be achieved by probing both the ambient and increased pressure cell populations for mitofusin protein levels.

While there are some studies available which look at the effect of knocking down mitofusin expression in cells, it is also important to take that into an animal model. Using the glaucoma mouse model, where mitochondrial function is compromised, allows us to study the mitofusins *in vivo*, where the altered mitochondria will be in an otherwise known environment. This will allow us to discover what role the mitofusins play in mitochondrial compromise in disease. Changes in the RGC axon seem to show an accumulation of mitochondria in bottleneck areas near the nodes. These mitochondria have undergone fusion, being morphologically much larger, and unable to pass through the bottleneck (Horner lab, unpublished data). With Mfn2 playing a necessary role in transport (Misko et al., 2010), it is certainly a possibility that both Mfn2 and Mfn1 are compromised in some way.

This leads to the hypothesis that disease-induced metabolic challenges and stressors create an imbalance of mitochondrial fusion and fission proteins in specific cellular compartments, which, in conjunction with compromised axonal transport, contributes to increased mitochondrial dysfunction.

Part II: Retinal ganglion cells accumulate a phosphorylated form of Mitofusin2 protein that correlates with glaucomatous disease progression.

Abstract

Glaucoma is a neurodegenerative disorder characterized by progressive deterioration of optic nerve (ON) and eventual death of retinal ganglion cells (RGCs). While age and elevation of intraocular pressure (IOP) are key risk factors in glaucoma, other events likely play a role in the loss of RGC viability. Decreases in axonal transport and bioenergetic vulnerability are key early features of glaucoma, though underlying mechanisms are unknown. We examined the correlation between bioenergetics and axonal transport with mitochondrial mutation frequency and posttranslational modifications of Mitofusin 2 (Mfn2) in RGCs during glaucoma progression. No increase in the frequency of mitochondrial DNA (mtDNA) mutations was detected, but we observed significant shifts in mitochondrial protein species. Mfn2 is a fusion protein that functions in mitochondrial biogenesis, maintenance, and mitochondrial transport. We demonstrate that Mfn2 accumulates selectively in RGCs during glaucomatous degeneration, that two novel states of Mfn2 exist in retina and ON, and identify a phosphorylated state that selectively accumulates in RGCs but is absent in ON. Phosphorylation of Mfn2 is correlated with increased ubiquitination of phosphorylated Mfn2, and failure of the protein to reach the ON. Together, these data suggest posttranslational modification of Mfn2 is associated with its dysregulation during metabolic changes preceding glaucomatous degeneration. Future work to manipulate either expression of Mfn2 or prevention of the degradation of Mfn2 could have therapeutic value in the treatment of glaucoma.

Introduction

Glaucoma is a neurodegenerative disease of the eye and optic nerve, characterized by RGC axonal degeneration and eventual RGC soma loss in the retina (Buckingham et al., 2008; Calkins and Horner, 2012). The underlying mechanisms that initiate the disease are just beginning to be elucidated. Considerable emphasis has been placed on neurodegenerative changes within the optic nerve, as they precede vision loss and ganglion cell death (Bosco et al., 2008; Calkins, 2012; Calkins and Horner, 2012; Morrison et al., 1997; Nguyen et al., 2011). At the earliest stages of glaucoma, axonal transport mechanisms are disrupted, interfering with

organelle transport, including mitochondria (Bosco et al., 2008; Misko et al., 2010). A key therapeutic question is whether early changes in the optic nerve transport mechanism and metabolic capacity can be targeted to slow or prevent neurodegeneration.

In glaucoma, RGC axons are compromised in many ways, including a decrease in ATP production and disruption of mitochondrial transport (Baltan et al., 2010; Knott et al., 2008). We have previously shown that the axons of DBA mice are more susceptible to metabolic challenges, with their ability to recover significantly compromised (Baltan et al., 2010). Our lab also showed that the mitochondria of healthy RGCs are typically short and punctate but become elongated or fused and tend to cluster more tightly around the nucleus during glaucomatous degeneration (Uo et al., 2009).

Loss of metabolic capacity and changes in mitochondrial morphology and location are accompanied by a disruption of axonal transport mechanisms typified by disrupted organelle transport, including mitochondria (Chen Y, 2011). Mitochondrial biogenesis, maintenance and morphology are regulated, in part, by a family of proteins that participate in the fusion and fission of membranes (Chan, 2006a, b; Chen et al., 2010; Huang et al., 2007).

A number of neurodegenerative diseases are associated with abnormalities in mitochondrial dysfunction. Defects in Opa1 (optic atrophy 1), an inner membrane fusion protein, cause increased mitochondrial fragmentation and severe cristae malformations (Song et al., 2009). Opa1 also acts to sequester pro-apoptotic cytochrome c molecules within the mitochondrial cristae spaces (Cipolat et al., 2006; Frezza et al., 2006). Genetic mutations in Opa1 cause autosomal dominant optic atrophy (DOA) (Davies et al., 2007), one of the most common inherited optic neuropathies, and is linked to other clinical manifestations, most commonly sensorineural deafness, ataxia, myopathy and progressive external ophthalmoplegia (Chen et al., 2003; Cho et al., 2010; Knott and Bossy-Wetzel, 2008; Yu-Wai-Man et al., 2010b).

Mutations of Mfn2 result in Charcot-Marie-Tooth (CMT) disease, the most common inherited neuromuscular disorder, and affects the motor and sensory neurons. More than 40 mutations of Mfn2 have been identified in CMT2A patients, with the majority of these mutations are missense mutations (Cho et al., 2010).

Drp1, a mitochondrial fission protein, causes mitochondrial fragmentation. If fragmentation shifts out of balance, it can contribute to synaptic damage and subsequent neuronal cell death. Emerging evidence suggests that impaired mitochondrial dynamics are

involved in the pathogenesis of Alzheimer's (AD) and Parkinson's disease (PD), with expression of levels of Drp1, Opa1 and Mfn1/2 significantly decreased in hippocampal neurons of human AD brains. Mitochondrial dysfunction has long been implicated in the pathogenesis of PD (Cho et al., 2010).

Recently, a new function for mitochondrial fusion proteins has been described that increases their potential relevance in the glaucoma. Misko and colleagues have demonstrated that Mfn2 is directly associated with Milton and Miro in dorsal root ganglion neurons, thus supporting Mfn2's role in mitochondrial transport. It was further demonstrated that the mitofusins are required for mitochondrial transport within axons and loss of Mfn2 results in severe transport deficits (Misko et al., 2010).

Given that Mfn1 and Mfn2 are both outer mitochondrial membrane proteins involved in fusing the outer membranes and are necessary for mitochondrial transport we sought to examine their potential relevance in glaucoma. One barrier to the study of these proteins has been the challenge of analyzing mitochondrial proteins from the small compartments of the visual pathway in diseased mice. We took advantage of a new nanoimmunoassay probe and optimized a novel method to measure low-abundance proteins as well as to begin to determine animal-to-animal variance of these proteins. The data indicate that a distinct splice variant and phosphorylation state of Mfn2 is upregulated early in the disease and it may thus be a unique harbinger of early metabolic dysfunction in glaucoma.

Methods

Animals

Experiments were conducted in accordance with regulations set forth in the Association for Research in Vision and Ophthalmology Statement for the Use of Animals in Ophthalmic and Vision Research, and were conducted under protocols approved by the Institutional Animal Care and Use Committees at the University of Washington (UW). DBA/2J (DBA/diseased) mice and DBA/2J^{Gpnmb+} (D2G/control) were initially obtained from Jackson Laboratories (Bar Harbor, ME), and bred and maintained at a pathogen-free facility in the UW vivarium at the South Lake Union facility, with new breeding pairs incorporated into the colony every year (Inman et al., 2006). All animals were kept on a 12-hour light/dark schedule with ad libitum access to food and water.

DBA/2J (DBA) mice are a well-established mouse model of glaucoma (Howell et al., 2007; John et al., 1998; Libby et al., 2005; Rangarajan et al., 2011). These mice have spontaneously developed two mutations (Anderson et al., 2002; Chang et al., 1999) resulting in the development of elevated IOP and glaucoma as they age, in a similar fashion as humans. In early stages (young), the DBA does not show outward manifestations of disease. This begins to change at five to six months, when the optic nerve begins to retract, sight is compromised, and there is metabolic deficit. In the late, chronic stage (aged), many RGCs are dead, the mice are blind, and ATP production is severely curtailed (Baltan et al., 2010; Buckingham et al., 2008; Inman et al., 2013; Lambert W, 2008).

The DBA/2J^{Gpnmb+} (D2G) mice are genetically identical, except they have only one of the two mutations, and do not develop glaucoma, thus act as the control for both disease and aging studies.

Age-matched animals were used in all experiments. Young animals were 3 months old; 6 month animals were 5-7 months; aged animals were 9-13 months.

Tissue preparation

Animals were anesthetized with Beuthanasia and the eyes were removed with the optic nerve still connected. The retina was removed from the orb, and the optic nerve was snipped free of the back of the eye. The brain was exposed in the skull and the superior colliculus region was excised. The tissues were collected, and snap frozen for future protein or RNA analysis as described below. Tissue collected for protein analysis was collected into tubes on dry ice, weighed, and ice-cold lysis buffer was added in w/v ratio of 5-10 ml lysis buffer per mg of tissue. Tissue collected for RNA analysis was placed into cold Trizol® and processed using the manufacture's protocol.

Mice were three to thirteen months old at the time of tissue collection. For RNA analysis, tissue from 3-7 animals were pooled together. Each n represents one pooled sample. For NanoPro analysis, each n represents one animal.

Immunohistochemistry

Retinal cross-sections were prepared by placing unfixed eyecups containing the retina, but not the lens, in Tissue-Tek® OCT compound and snap freezing with liquid nitrogen. Frozen

tissue was then sectioned on a Leica CM1850 cryostat (10 mm thick) and collected and dry mounted on Fisherbrand Superfrost/Plus slides. Slides were stored at -80°C until used. Slides were rinsed, blocked, and incubated with primary antibodies, blocked again, and then incubated with secondary antibodies. DAPI was applied prior to coverslipping.

Primary antibodies were applied in the following concentrations: anti-Mfn1 (chicken, 1:250, Novus), anti-Mfn2 (rabbit, 1:1000, AbCam), anti-NeuN (mouse, 1:1000, Chemicon), anti- ChAT (goat, 1:500, Chemicon), anti-GFAP (guinea pig, 1:250, Advanced ImmunoChemical) all diluted in blocking solution (0.4% Triton X, 5% donkey serum in Tris Buffer). To visualize primary antibodies a secondary antibody conjugated to redX, cy2 or cy5 was applied at a dilution of 1:250 in blocking solution as above. Nuclei were labeled with DAPI (1:1000, Sigma) just before coverslipping.

Protein sample analyses

Retina, optic nerve and superior colliculus were removed from mice that had been lethally anesthetized. Tissue samples were immediately placed into tubes being stored on dry ice. Tubes were weighed prior to and after the addition of the tissues to determine tissue weight, and maintained on dry ice. For every mg of tissue, 5-10 ml of ice-cold Bicine/CHAPS lysis buffer (with protease inhibitors and DMSO freshly added) was added to the tube. Tissue was broken down using pipette tips to homogenize the mixture and spun to remove cellular debris. The supernatant was placed to a fresh, chilled microcentrifuge tube. Lysate concentration was determined using BCA assay. Lysates were frozen and stored at -20 °C until used.

For use in nanoimmunoassays (O'Neill et al., 2006), lysates were diluted to a final concentration of either 0.05 mg/ml (retina, superior colliculus (SC)) or 0.1 mg/ml (ON) using SERVALYT^{TM} 4-7 carrier ampholyte and resolved by capillary isoelectric focusing electrophoresis using the NanoPro 1000 (ProteinSimple) according to our developed protocols (Nivison, ProteinSimple Application Briefs #1032, #1033, 2012). Resolved proteins were immobilized using UV crosslinking, then probed with primary antibodies in the following concentrations: α-Mfn1 (rabbit, 1:300, Santa Cruz), α-Mfn2 (rabbit, 1:25, Sigma); α-Ubiquitin (rabbit, 1:50, Cell Signaling). Secondary antibodies (ProteinSimple) used include: goat α-rabbit biotin conjugate (1:100) and streptavidin-HRP (1:100). Luminol/Peroxide XDR was used for signal detection.

Phosphorylation-specific states were identified using the Lambda Protein Phosphatase assay (Millipore), which was applied to protein samples and incubated for 30 minutes at 37° prior to being run on the NanoPro (NP).

Calculations of peak areas were done using Compass 1.8.1 (ProteinSimple).

In western blots, protein detection was performed using the same primary antibodies as above, as well as β-actin (rabbit, 1:1000 Cell Signaling). Secondary antibodies used include donkey α-rabbit HRP (Jackson, Amersham).

Quantitative reverse transcription-PCR

Whole retinas, optic nerves, and the superior colliculus regions were removed from DBA and D2G mice, and RNA was isolated and amplified as described above. Prior to running the RT-PCR, cDNA was prepared from the extracted RNA. The cDNA from pooled tissue samples were probed with FAM-labeled primers for Mfn1, Mfn2 and GAPDH, a housekeeping gene used for normalization. All quantitative reverse transcription PCR (qRT-PCR) was performed in triplicate using three separate pools of each tissue type under standard cycling conditions for FAM-labeled primers. The accompanying software for the Rotor-Gene 6 was used to visualize the data. Final analysis of the data was completed using an Excel spread sheet.

DNA isolation

To obtain whole DNA from mouse tissue, tissue samples were immersed in 1 mL homogenization medium (0.32 M sucrose, 1 mM EDTA, 10 mM Tris-HCl, pH 7.8) and disrupted with a glass Dounce-type homogenizer. The homogenate was transferred to a 1.5 mL tube and centrifuged at 13000 g. The pellet was re-suspended in 600 μL lysis buffer (10 mM Tris-HCl, pH 8.0, 150 mM NaCl, 20 mM EDTA, 1% SDS, and 0.2 mg/ml Proteinase K) and incubated at 55°C for 3 hr. DNA was isolated by phenol-chloroform extraction followed by isopropanol precipitation.

mtDNA Random Mutation Capture assay

The method for quantification of random mtDNA mutations was performed as detailed previously (Vermulst et al., 2008), with alterations to enhance throughput, outlined below. DNA was diluted and digested with 100 units TaqαI restriction enzyme (New England Biolabs), 1X

BSA and a TaqαI-specific digestion buffer (10 mM Tris-HCl, 10 mM MgCl2, 100 mM NaCl, pH 8.4) for 5 hrs, with 100 units TaqαI added each hr. Mutation frequencies at sites in the 12S rRNA and ND5 genes were determined via real-time PCR with primers flanking a TaqαI restriction site to quantify the number of mutant molecules, i.e., those molecules resistant to digestion. Real-time PCR was also performed with a set of control primers in a region without a TaqαI restriction site to quantify the total number of molecules. Standard curves were included to determine the relationship between copy number and cycle threshold for each primer set, and the resulting formulae were used to quantify target DNA in each well. Real-time PCR was performed in duplicate in 25 μL reaction volumes, with 12.5 μL 2x GoTaq Hot Start Colorless Master Mix (Promega) supplemented with SYBR Green I Nucleic Acid Stain (Lonza) at 0.2X final concentration, 500 nM each of forward and reverse primers, and diluted TaqαI-digested DNA. Reactions were thermally cycled on a CFX96 instrument (Bio-rad) with the following conditions: 37˚C for 10 minutes, 95˚C for 10 minutes, and 45 cycles of 95˚C for 30 seconds, 65˚C for 1 minute, and 72˚C for 90 seconds, followed by 72˚C for 5 minutes and a 4˚C hold. Mutant molecules were verified by a post-PCR TaqαI digest and agarose gel electrophoresis.

Imaging

Immunohistological images were visualized with a Zeiss Axioskop2 plus microscope with an Optronics camera. Confocal images were captured with a Nikon A1R microscope and 3D image stacks were further analyzed using Imaris 7.5 software (BitPlane, Zurich, Switzerland). Quantitative analysis of the confocal images was done using Imaris MeasurementPro and ImarisCell to identify RGC nuclei and mitochondrial surface protein Mfn2, and to measure both Mfn2 proximity to the nuclei and its abundance in the cell soma.

ImarisCell examines complex relationships between cells, between cell components, or of components within a cell. Statistics are generated on a per cell basis based on spatial relationships within a cell. Components are color coded to show in a visual manner complex relationships between cell components. Imaris MeasurementPro extracts statistical parameters from microscopy images for quantification by using object detection features to measure distances, and classifies the results based on calculated statistical parameters. Analysis is performed on a per cell basis on the combination of objects that meet selected criteria. In this case, distance between the nucleus and Mfn2-tagged mitochondria was set for 4 μm as defining

the perinuclear space, with Mfn2 tags falling outside this parameter not quantified. To eliminate background staining, only Mfn2 fluorescent signal of 4 pixels or greater were included in the analysis.

Statistical analysis

All data in this study are expressed as the mean ± SEM, except where otherwise indicated. Correlation coefficients, corresponding p values, and outliers were calculated using GraphPad Prism 3.0 (GraphPad Software, San Diego, CA) and Prism 6.0. Groups were compared using ANOVA with Welch's correction assuming a nonparametric comparison, ANOVA, two-way ANOVA, and unpaired t-tests.

Results

Mitochondrial DNA mutation frequency

It has been suggested that oxidative stress, induced by defective mitochondria, leads to an increase in mtDNA mutagenesis, and ultimately plays a causal role in the onset of glaucoma (Chrysostomou et al., 2013; Jarrett et al., 2013). In order to determine the relationship of mitochondrial DNA mutations to the pigmentary glaucoma phenotype, we measured the random mutation frequency in tissues from 9 month old control D2G and diseased DBA mice using the random mutation capture (RMC) assay (Bielas and Loeb, 2005) adapted for mtDNA (Vermulst et al., 2007; Vermulst et al., 2008). When evaluating separate tissue types affected by glaucomatous degeneration and thus expected to sustain an increased mutation burden (optic nerve, retina, and superior colliculus), we found no significant differences in mtDNA mutation load between D2G and DBA tissues when assessed individually at two mutation sites (Fig. 2.1a, 2.1b). These data indicate mitochondrial mutation frequency is not likely a contributing factor to declining mitochondrial function in the DBA model of pigmentary glaucoma.

Protein and RNA levels change with disease

We next sought to determine if either damage or dysregulation of proteins involved mitochondrial transport and morphology are present in glaucoma. Previous studies have shown that mutations of Opa1 cause disruption of fusion, resulting in DOA (Amati-Bonneau et al., 2008; Davies et al., 2007; Nguyen et al., 2011). Here we focused on two fusion proteins which

have not been fully analyzed for their role in neurodegenerative disease. The mitochondrial fusion proteins Mfn1 and Mfn2 play important roles in mitochondrial behavior. In this study, we looked at both RNA and protein levels of Mfn1 and Mfn2. In assessing RNA levels, it was necessary to use pooled tissue from retina, optic nerve and superior colliculus (data not shown) from three age-matched DBA and D2G control animal cohorts to acquire enough tissue for analysis. Each pooled sample contained tissue from three to seven animals. We found RNA expression of Mfn1 did not change significantly in the retina of control and diseased animals at 3, 6 or 9-12 months of age (Figure 2.2a). Mfn2 RNA expression did not change across retinal tissue in either D2G or DBA, but levels were significantly decreased in DBA cohorts at 3 months ($p = 0.0106$) and 9 months ($p = 0.0424$). Overall Mfn2 RNA expression was decreased in the DBA animals ($p = 0.005$) when compared with the D2G controls (Figure 2.2b). Two-way ANOVA confirms condition is statistically significant ($p<0.0001$) and interaction between age and disease is significant ($p=0.0349$).

Mfn1 RNA expression in the ON had an upward trend that correlated with age in the D2G animals but was not significant. The opposite trend was observed in DBA animals and became significantly decreased in the 6 month cohort ($p = 0.0172$, Figure 2.2c). Mfn2 RNA expression trended downward although it did not change significantly in the DBA ON at any time point (Figure 2.2d, $p = 0.0644$). Because of the need to use pooled tissue to conduct these assays, we predicted that small changes could be diluted by inter-sample variability and the significance of the observed trend could be better confirmed using a more sensitive method.

We have previously reported changes in mitochondrial protein by western blot in DBA animals (Uo et al., 2009). These data indicated increased Mfn1 and Mfn2 in DBA mice during aging that was significantly different compared to age-matched B6 controls. We also observed a natural, age-related decline for both fusion proteins in B6 control mice. In the current approach we sought to reassess these data using tissue from D2G mice, the optimal genetic control. The D2G mouse does not develop glaucoma, but is in all other ways genetically similar.

Mfn1 levels are lower in D2Gs when compared with diseased DBA animals (Figure 2.2c'). These data are similar to our previously published findings using the B6 mice as controls (Uo et al., 2009). In contrast, we detected decreased Mfn1 with age in both control and glaucomatous mice (Figure 2.2c'). Similar to the earlier study, we found Mfn2 protein levels were higher overall in the DBA retina (Figure 2.2b') when compared with D2G controls, and

showed an age-related decline in D2G and age-related increase in DBA. The similarity in findings for the D2G mice confirms the appropriateness of using them as controls, eliminating any question that genetic variability alone is the cause of observed protein changes.

In using the genetic controls, we were able to confirm elevated levels of Mfn2 in retina, which indicates that retinal Mfn2 is increasing and thereby may indicate an increased demand for mitochondrial fusion or transport.

IHC shows Mfn2 accumulation in RGCs

Immunohistological staining for Mfn2 in retinal cross-sections was assessed to determine how Mfn2 protein is distributed during disease progression. We found Mfn2 is concentrated in RGCs and accumulates more rapidly in the surviving RGCs during disease progression (Figure 2.3).

Confocal imaging of 3 month old retina shows even distribution of Mfn2 immunoreactivity throughout the retina but is particularly concentrated in NeuN-positive RGCs. The inset shows the proximity of the Mfn2 to the nuclei. However, ten month old DBA retina had decreased Mfn2 levels (Figure 2.3c), as well as fewer RGCs overall, while the inset shows an increased accumulation of Mfn2 in close proximity to the nuclei.

We used Imaris imaging software to localize Mfn2 protein to intracellular structures and quantify total immunoreactivity in individual cells. Mfn2-tagged mitochondria were particularly concentrated in the cytoplasm surrounding the nucleus of the RGC. We found that the number of RGCs and the amount of Mfn2 labeling decreased during aging in the DBA. The distribution of Mfn2 indicates that young DBAs have uniform protein that is primarily localized to perinuclear region of the RGCs (Figure 2.3b). In aged DBA, there was a noticeable increased accumulation of Mfn2 in the perinuclear space on a per-cell basis (Figure 2.3d). While not directly measured, Mfn2 levels in the remaining retinal layers appeared constant. These data suggest that Mfn2 and mitochondria remain near the somal compartment with fewer transporting along the axon during disease progression.

We next quantified the intracellular distribution of Mfn2 protein. We found that Mfn2 protein within 4 mm of the nucleus in aged, disease RGCs is two-fold higher than that found in young DBA (Table 2.1). The number of NeuN+ cells (RGCs) in aged disease retina is significantly decreased when compared to young retina ($p=0.0034$) or aged control retina ($p =$

0.0416). The amount of Mfn2 protein in aged disease is significantly decreased when compared to young retina ($p = 0.0223$), although not significantly different from aged control retina. The amount of Mfn2 protein detected within the perinuclear space of the aged disease RGCs is significantly increased over both the young RGCs ($p = 0.0171$) and the aged control RGCs ($p = 0.0178$).

The increased ratio of Mfn2 per RGC in the diseased DBA may explain the western blot data where we detected only modest decreases in protein. Together, these data indicate that as RGCs are degenerating, Mfn2 protein is accumulating within the perinuclear space of the surviving nuclei at an increased rate. The colocalization of Mfn2 with mitochondria near the nucleus implies decreased degradation or dysfunctional circulation of mitochondria. If this is confirmed to be a transport dysfunction for mitochondria, it could have a significant impact on the cells' energy state.

Development of a quantitative nanoimmunoassay for small amounts of protein

The need to pool tissue from multiple animals to conduct the protein and RNA assays limited the ability to adequately evaluate changes occurring with Mfn1 and Mfn2 protein expression on an individual animal level. Pooled samples made it particularly difficult to dissect out changes to the phosphorylated state or splice variants of the protein. We sought to further characterize changes to Mfn2 and specifically look for post-translational or active kinase activity of Mfn2 during disease progression.

To accomplish this we developed nanoimmunoassays capable of detecting signals from between 0.05 and 0.1 mg/ml of total protein. Using a capillary isoelectric focusing electrophoresis nanoimmunoassay (NanoPro), we were able to observe differences in both Mfn1 and Mfn2 in individual disease and control animals.

NanoPro is best described as a cross between a western blot and an ELISA which occurs in a capillary, with proteins separated by an isoelectric gradient. Cell or tissue lysates are mixed with standards in a sample buffer that creates the gradient. An electrical field separates the proteins by their isoelectric points. The proteins are then immobilized at different locations along the length of the capillary and can then be probed by primary and secondary antibodies. Ultimately applying a chemiluminescent signal allows the results to be measured and quantified.

In the development of the assay, the consistency of the peaks which arise for Mfn2

demonstrate the protein's position in relation to the standards in the buffer (Figure 2.4a). In the Mfn2 assay, these peaks occur at the approximate isoelectric points (pI) of 6.2 and 6.5, the latter of which corresponds to the hypothetical isoelectric point (6.52) for Mfn2, further confirmation that these peaks represent Mfn2 protein. Other spikes arise, but not consistently, thus proving to be solely background noise. Also in the process of developing the assay, control cells and control antibodies are tested. The small, lower tracings in the inset (Fig. 4a') show ERK levels in HeLa cells, with the upper tracings showing ERK in retinal tissue. Baselines and areas under the curves (peaks) are calculated by the proprietary software, Compass.

Upon determining the actual Mfn2 peaks, changes to protein levels attributable to age or disease can then be measured. In figures 4b-e, replicate tracings focusing in on individual conditions in retinal tissue reflect changes in Mfn2 protein, with 4b showing young control (D2G) levels, 4c shows young disease (DBA) levels, 4d shows aged D2G levels, and 4e shows aged DBA levels. The percentages reflect the average amount of protein in each of the peaks in each of the conditions.

Nanoimmunoassay shows a phosphorylation-specific peak in Mfn2 that selectively increases in glaucomatous retina

The analysis began by comparing healthy and diseased tissues at two different ages, to expose changes due to age as opposed to disease. Protein analysis performed by NanoPro revealed two Mfn2 peaks in both ON and retina. These data indicate that Mfn2 is resolved into the two defined peaks with slightly different isoelectric points (see Figure 2.4).

In an effort to distinguish the two peaks, a phosphatase-stripping assay (Lambda Protein Phosphatase Assay, Millipore) was performed on the lysates. This created a near-complete depletion of the 6.2 peak in both tissues (Figure 2.5a, 2.5b) with a concurrent increase in the second 6.5 peak, indicating that there is an active, phosphorylated form of Mfn2 present. This shift to the non-phosphorylated form is not due solely to aging (Figure 2.5c), but, rather, occurs in diseased animals (Figure 2.5d). Recent work in heart tissue has uncovered two phosphorylation sites on Mfn2 (Eschenbacher et al., 2012). These data now demonstrate that Mfn2 is reversibly phosphorylated in neuronal tissue.

When quantifying this shift in control and disease animals, there were significant decreases in overall peak size, as well as the loss of the 6.2 pI peak in diseased tissue. In young

DBA mice, the phosphorylated Mfn2 was found to be already elevated compared to age-matched D2G. These data indicate that the phosphorylated form of Mfn2 may be a novel indicator of disease progression. As DBA mice age and exhibit elevated intraocular pressure and degenerative disease, there is a significant increase in unphosphorylated Mfn2. In contrast, in control animals at both 3 months and 10 months, the ratio of phosphorylated and unphosphorylated Mfn2 is close to one.

Mfn2 protein levels increase significantly in glaucomatous retina but decrease in effected optic nerve

Using the NanoPro to further assess mitofusin protein levels, we found that young and aged tissue express Mfn2 differently. In both young DBA optic nerve and retina, Mfn2 is expressed at significantly higher levels than when compared to young controls (Figure 2.6a, 2.6b). However, in the aged optic nerve (Figure 2.6c), a dramatic, 3-fold decrease in the amount of Mfn2 is seen in control tissue when compared to disease tissue levels. This is in juxtaposition to the finding in the aged retina (Figure 2.6d), where Mfn2 level in disease shows a three-fold increase when compared with age-matched controls. Quantifying these differences underlines the highly significant changes in disease (Figure 2.6e, 2.6f).

The dramatic decrease in Mfn2 levels in the disease optic nerve, coupled with a significant increase in the diseased retina, suggests that Mfn2 may be accumulating in the soma. Declining levels of Mfn2 in the optic nerve could indicate that Mfn2 protein is not being transported down the axon to where it normally functions in mitochondrial transport and repair.

Another observation is the relative change in peak sizes that correlate with disease progression (Figure 2.6b, 2.6d). In control animals of both age groups, both Mfn2 peaks are of similar size, indicating the presence of similar amounts of the two Mfn2 forms. In young DBA retina, there is a greater amount of phosphorylated Mfn2 present (the 6.2 peak), while there is a shift to an increase in the dephosphorylated Mfn2 state (6.5 peak) in the older, diseased retina.

In contrast, but in agreement with our protein analysis, Mfn1 shows similar expression patterns and levels in both control and disease ON (Figure 2.7a). While the quantification of total Mfn1 protein levels shows a significant ($p = 0.0118$) decrease with aging, there is no difference between control and disease (Figure 2.7b). However, when broken down by individual peak area, there is a major shift from the phosphorylated peak (P1) to the non-phosphorylated peak (P2)

that occurs with age ($p = 0.013$) (Figure 2.7c).

In the retina, Mfn1 levels in retina were not consistent between control (D2G) and diseased (DBA) animals. Control animals show a dramatic drop in Mfn1 levels as they age (Figure 2.7d, 2.7g, $p = 0.0034$), while, conversely, DBA animals express significantly higher levels of Mfn1 at as they age (Figure 2.7e, 2.7g, $p = 0.0022$). Mfn1 expression levels in 13 month D2G retina decreased in comparison to 11 month DBA retina (Figure 2.7f, 2.7g, $p = 0.0036$). The rise in Mfn1 levels that occurred with age was seen solely in the DBA animals, with Mfn1 decreasing with age in controls (Figure 2.7g). In the aged animals, the disease animals express significantly higher levels of Mfn1 ($p = 0.0036$). Thus, in the retina, Mfn1 protein levels reflect an inverse expression pattern between control and DBA animals with age ($p < 0.002$).

Others have shown that Mfn1 can act in a compensatory fashion when Mfn2 levels are compromised (Chen et al., 2007; Misko et al., 2010). These data show that no compensatory increase in Mfn1 occurs in either the optic nerve or the retina of glaucomatous animals. The increase of Mfn1 observed in diseased retina mirrors the increase occurring in Mfn2. There are no changes in Mfn1 levels between control and disease animals in optic nerve.

Ubiquitin levels decrease in retina with disease progression

Ubiquitin is a post-translational modification that is used to tag dysfunctional mitochondria for degradation (Whitworth and Pallanck, 2009). Assessing protein levels of ubiquitin in retina showed that ubiquitin levels remain stable in control animals (Figure 2.8a), but decline dramatically with disease progression (Figure 2.8b). There was no difference in levels in the young DBA animals prior to disease onset. We did find a significant decrease in ubiquitin levels in aged, diseased retina. Through immunoprecipitation, we were able to determine that ubiquitin is associated with Mfn2 in retinal tissue (Figure 2.8c). When examining ubiquitin levels through Western blot (Figure 2.8d), we found a similar decrease in ubiquitin levels in the disease retina, with no change in controls over time.

In the ON, ubiquitin levels decrease with age in both control and diseased mice. We were unable to detect ubiquitin in the optic nerve using the NanoPro (data not shown). This limits our ability to know whether ubiquitin is absent in the NanoPro preparation or at levels below the detection limit. Ubiquitin was detectable by Western blot, where pooled samples of ON from 6 to 8 animals were used, suggesting that levels are low in individual animals.

Discussion

Glaucoma is a condition marked by disrupted energy balance (Baltan et al., 2010), transport deficits (Buckingham et al., 2008) and changes in mitochondrial form and function (Nguyen et al., 2011). Hence, there is collective evidence for mitochondrial dysfunction that could be a result a direct dysregulation of mitochondrial dynamics and transport due to glaucomatous disease. Alternatively, mitochondrial dysfunction could result from indirect damage of proteins or DNA due to oxidative stress and inflammation. One hallmark of an indirect oxidative effect would be damage to mitochondrial DNA, which has been observed in a sample of patients with congenital glaucoma (Tanwar et al., 2010).

The role mitochondria play in neurodegenerative disease as an initiator and arbiter or a secondary phenomenon remains unknown. Here we sought to determine if an increased mtDNA mutation frequency underlies the ATP crisis and metabolic vulnerability that we have previously described in DBA tissue (Baltan et al., 2010). Since there has not been a defined single mutation that results in glaucoma, especially one that is associated with nuclear mitochondrial genes, we analyzed the frequency of mtDNA mutations in optic nerve, retina, and superior colliculus from glaucomatous DBA mice. No significant differences in mtDNA mutation burden were observed between D2G and DBA mouse tissues (Figure 2.1). Collectively, these data suggest that mtDNA mutation, thought to result from increased oxidative stress or inflammation, does not underlie the mitochondrial dysfunction in glaucoma. Hence, we focused our subsequent work on the analysis of key mitochondrial regulatory proteins important in their mobility, biogenesis and repair.

A family of fusion and fission proteins has recently garnered significant interest in multiple aspects of mitochondrial function. There has been a much greater focus on the various fission proteins and their role in disease compared to fusion proteins (Elgass et al., 2013; Youle and van der Bliek, 2012). Due to the purported role of fusion proteins in mitochondrial docking and transport (Chen et al., 2003; Huang et al., 2011; Misko et al., 2010), and the limited description of their role in glaucoma, we chose to focus on Mfn1 and Mfn2. Protein analysis in pooled tissue assays demonstrated that changes in levels of the mitofusins occur as disease progresses. While this method allowed us to observe overall trends associated with age and disease, we only detected a disruption of retinal Mfn2 that reached significance. We proposed that the complex architecture of the visual system and multiple cell types could dilute the

measurement of potentially key mechanistic findings. To solve this problem, we developed a nanoimmunoassay which is sensitive enough to evaluate very small quantities of protein (Frogne T, 2012; O'Neill et al., 2006). This is essential for detecting low abundance protein in limited tissue samples such as optic nerve and, thus, allows for single-animal assessments. We devised assays for Mfn1, Mfn2 and ubiquitin. This additional sensitivity determined that Mfn2 is more dynamic than Mfn1 in a model of glaucoma, perhaps because of Mfn2's additional role in mitochondrial transport (Misko et al., 2010). It also showed that changes in the superior colliculus were less dynamic than that of retina or ON tissue.

In ON, Mfn1 protein expression pattern and levels are the same, while in retina, the pattern is reversed. In Mfn2, protein levels increase dramatically and significantly in disease retina while decreasing similarly in disease ON (Figure 2.9). Mfn1 has been shown to have a rescue effect in circumstances in which Mfn2 is compromised (Chen et al., 2003; Chen et al., 2007; Misko et al., 2010). In this compensatory role, one would expect to see an upregulation of Mfn1 in instances where Mfn2 is not present or present at diminished levels. As is shown by the graph (Fig. 9), Mfn1 does not compensate for the loss of Mfn2 seen in the ON. The only region we see significant changes in Mfn1 is in the retina where protein levels diminish with normal aging but remain unchanged during disease. However, it does not appear that Mfn1 is increasing in compensation of decreasing Mfn2, as Mfn2 also increases in retina with disease progression. Importantly, we found optic nerve Mfn2 levels significantly changed between the healthy and diseased animals at both young and older ages. This is in contrast to stable Mfn1 levels. Thus, the dynamics between Mfn1 and Mfn2 are not solely of a compensatory nature, with Mfn2 levels changing more significantly, particularly in the optic nerve where transport is ongoing.

In glaucoma, RGC axons are compromised in many ways, including a decrease in ATP production and disruption of mitochondrial transport (Baltan et al., 2010; Knott et al., 2008; Lee et al., 2011). In our lab, we have previously shown that the axons of DBA mice are more susceptible to metabolic challenges, with their ability to recover severely compromised. Mfn1 and Mfn2 proteins are located in the outer mitochondrial membrane and are directly involved in mitochondrial fusion, as well as transport of the mitochondria up and down the axons. Our lab has shown previously that mitochondria in normal RGCs are short and punctate, while those in glaucomatous neurons are elongated or fused and tend to cluster more tightly around the nucleus.

We have also detected a decrease in mitochondrial number in glaucomatous axons, potentially indicating a failure of transport (Uo et al., 2009). In the current research, we utilized image analysis to demonstrate that Mfn2 accumulation is localized to the perinuclear space of glaucomatous RGCs. We also demonstrated that, while overall Mfn2 levels decrease, the amount of Mfn2 in surviving RGCs increases. Together with our observation of decreased Mfn2 expression and protein in the DBA optic nerve, we postulate that adequate Mfn2 protein exists in the retina but the protein is either damaged or fails to transport to the optic nerve. A better understanding of this mechanism could be pivotal for establishing the role of Mfn2 function in the axon transport deficits and metabolic crisis that coincides with glaucoma.

Mfn2 exists in an active and inactive state that is phosphorylation dependent (Chen and Dorn, 2013). Mfn2 is phosphorylated by PINK1 on T111 and S442 in models of PD, and mutations at these sites alter mitochondrial dynamics. Phosphorylated Mfn2 is a receptor for Parkin on depolarized mitochondria in cardiac tissue (Chen Y, 2011). In this study, we are able to demonstrate for the first time that Mfn2 has at least one active phosphorylation site in the central nervous system. In addition, we detected two modifications that can be resolved by their isoelectric point as separate protein peaks. The smaller isoelectric point corresponds to the phosphorylated Mfn2 present in the tissue. We found the amount of phosphorylated Mfn2 to be greater in young DBA mice when compared with the age-matched controls. These data indicate that Mfn2 phosphorylation decreases during normal central nervous system aging. Interestingly, we detected a significantly larger loss of phosphorylated Mfn2 during disease progression. Decreased and delayed axon transport is observed in cultured dorsal root ganglions that lack Mfn2 (Misko et al., 2010) and is not a part of normal aging. Since Mfn2 requires active phosphorylation to bind to kinesin, impaired phosphorylation could impede organelle transport. Alternatively, lowered ATP availability or damage to Mfn2 would also prevent phosphorylation of Mfn2 and subsequent interaction with kinesin. The end result would be similar to the transport deficits that arise in glaucoma. The transport malfunction being attributable to Mfn2 dysregulation is further strengthened by our IHC findings of Mfn2 localized most heavily around the nucleus of the RGC, and not widely diffused throughout the axonal processes. Alternatively, mitochondrial fusion also consumes ATP, and this process would be compromised in the presence of unphosphorylated Mfn2, low Mfn2 availability or damaged Mfn2 protein. Deficits in mitochondrial fusion impede mitochondrial repair and function (Chan, 2006a, b, 2012; Chen Y,

2011; Cho et al., 2010). Future research is needed to understand the temporal dynamic whereby unphosphorylated Mfn2 does not function properly, contributes to transport disruption, mitochondrial dysfunction and underlying neurodegeneration.

In drosophila, ubiquitin is recruited to the mitochondrial outer membrane via the Pink/Parkin pathway when membrane depolarization occurs (Poole et al., 2008). One of the triggers for this recruitment is the depolarization of the outer mitochondrial membrane, the first step in mitophagy (Glauser et al., 2011; Poole et al., 2010), with translocation of Parkin to the mitochondria for degradation (Gegg et al., 2010; Tanaka et al., 2010). Thus, we next determined whether ubiquitin is recruited to Mfn2, where it could interfere with Mfn2's role in transport. We found that ubiquitin does colocalize with Mfn2, but not Mfn1 (data not shown), and that it is more highly present in young DBA animals. This allows one to hypothesize that the loss of ubiquitinization of Mfn2 prevents repair and recycling of the protein which could interfere with both mitochondrial fusion and transport.

These data implicate a loss of function of Mfn2 and its altered phosphorylation state in the measured, metabolic dysfunction and transport and mitochondrial fusion changes observed in many forms of glaucoma. In the future, we can begin to address potential targets for correcting mitochondrial behavior and health and also explore the exciting possibility that changes in fusion protein status could serve as a useful biomarker for axonal degeneration. In addition, what we can learn about mitochondrial compromise in this specific neurodegenerative disease may well translate to other "long axon" diseases (Chan, 2006b). Mitochondrial disruption is an early event in neurodegeneration, with impaired bioenergetics and migration acting as neurodegenerative triggers (Knott et al., 2008). As mitochondria play so many key functional roles in the cell, the decrease of ATP production and disruption of mitochondrial transport can readily be viewed as a pivotal cause underlying disease (Baltan et al., 2010). Conversely, disease may interfere with the cellular infrastructure, disrupting mitochondria's ability to function in its many necessary locations throughout a cell. In either case, the ability for mitochondria to function properly and disease are incontrovertibly linked (Detmer and Chan, 2007). Therapeutically manipulating the balance between fusion and fission proteins may improve recovery or delay axonal degeneration.

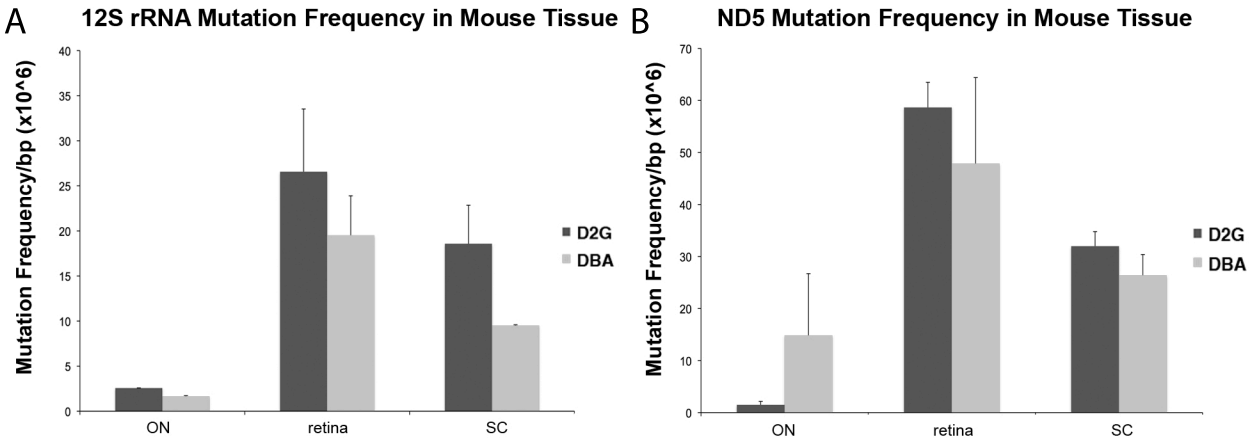

Figure 2.1. Mitochondrial DNA mutation frequencies in diseased tissue do not differ from those in healthy tissue. Evaluating separate tissue types affected by glaucomatous degeneration, we found no significant difference in mutation burden between control D2G tissues and DBA tissues at either the A) 12S rRNA or B) ND5 loci in mitochondrial DNA.

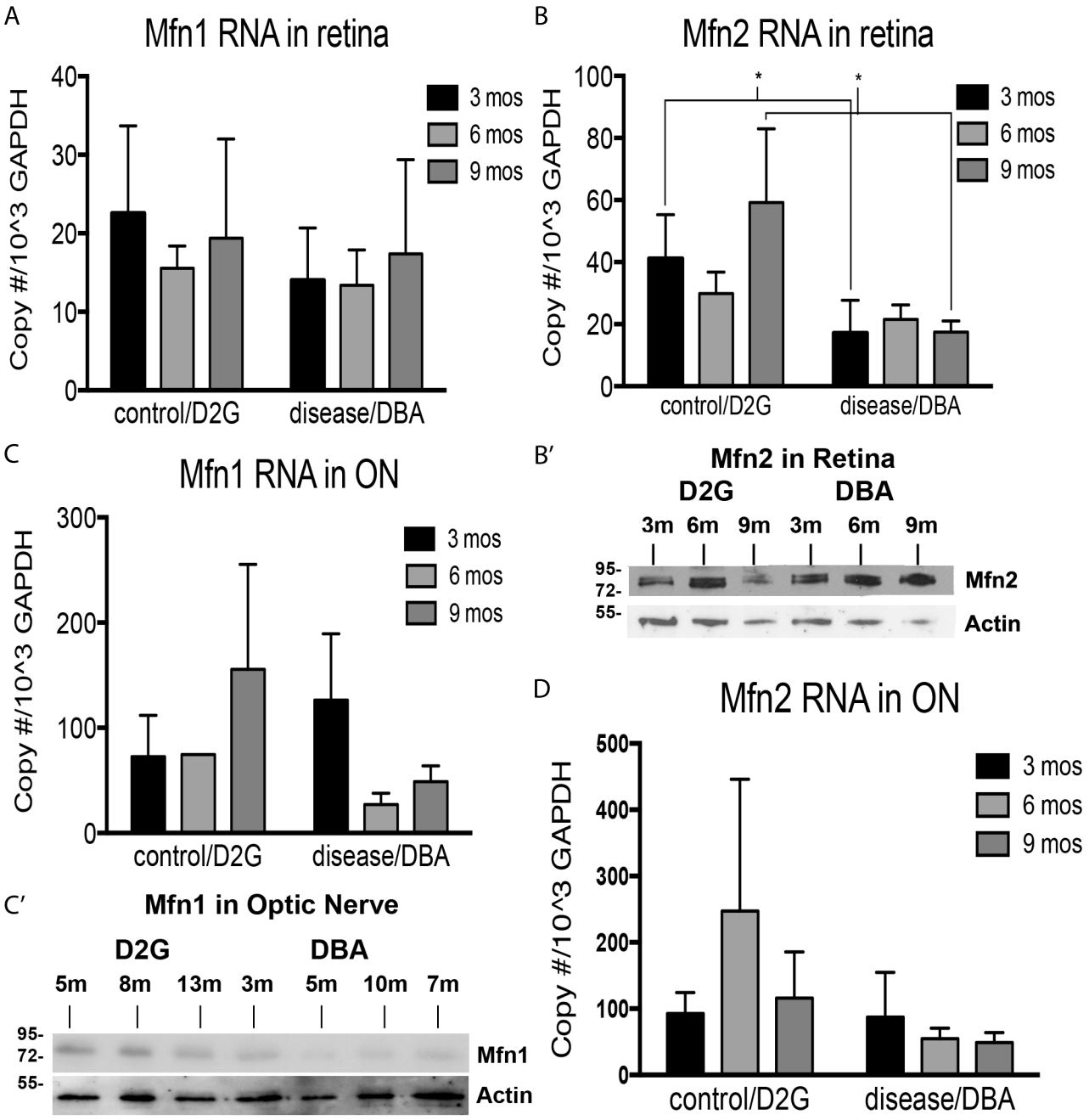

Figure 2.2. Protein and RNA levels change with disease progression. A) RNA expression of Mfn1 is steady in retina in both control (D2G) and diseased (DBA) animals over all ages, while B) Mfn2 RNA expression in retina is steady in D2Gs and DBAs, but significantly lower in the DBA animals at both 3 months (* $p = 0.0106$) and 9 months (* $p = 0.0424$); overall expression is significantly greater in the controls when compared to the DBAs ($p = 0.005$). C) In ON, Mfn1 RNA expression trends toward increased expression with age in D2Gs, while decreasing with age in the DBAs, with the decrease reaching significance between the 6 month cohorts ($p = 0.0172$). D) Mfn2 RNA expression does not change significantly in ON, although the decreased expression in the DBAs approaches significance ($p = 0.0644$). A') Immunoblot shows higher levels of Mfn1 in control retina when compared with disease tissue and B') with overall higher levels of Mfn2 protein in the diseased retina.

n= number of separate pooled samples of 3-7 animals. In ON, n=3, except 3m DBA, where n=4. In retina, n=3 in 6m Mfn1 cohorts; n=4 in 6m and 9m D2G Mfn2; n=5 in 3m and 9m D2G, and 3m DBA Mfn1, and 3m D2G, 6m and 9m DBA Mfn2; n=6 in 9m DBA Mfn1 and 3m DBA Mfn2.

Significance was determined using unpaired t-test with Welch's correction. * $p < 0.05$. Two-way ANOVA confirms condition is statistically significant ($p<0.0001$) and interaction between age and disease is significant ($p=0.0349$).

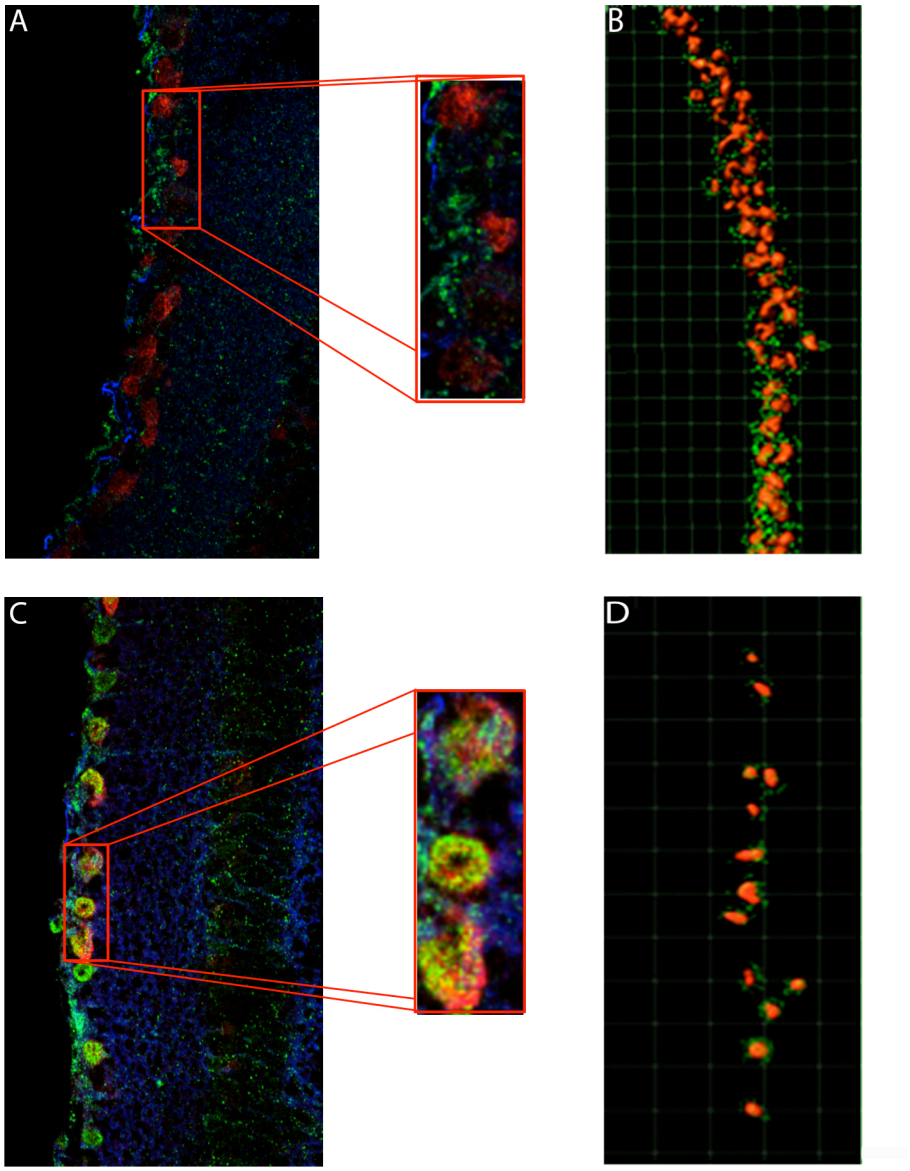

Figure 2.3. Mfn2 is concentrated in RGCs, with additional accumulation in degenerating RGCs. A) Immunofluorescent image of 3 month old retina shows expression of Mfn2 throughout the retina. Note that Mfn2 (green) can be seen to concentrate in NeuN positive RGCs (red) but is limited in other cells and layers of the retina. B) Imaris imaging shows distribution of Mfn2 in RGCs of young DBA2 have uniform protein primarily localized to RGCs. C) Image of a 10 month old retina shows a decreased RGC population. D) Imaris imaging of aged retinas show decreased NeuN (decreased RGC population) but increased accumulation of Mfn2 in the perinuclear space on a per-cell basis.

Table 1.

Age	# NeuN+	Mfn2	Nuclear proximity (4μm) of Mfn2
young DBA	54 ± 6.2	768 ± 87.8	14.2 ± 1.6/nucleus
aged DBA	14 ± 1.6 **	406 ± 47.6 *	29.0 ± 3.4/nucleus *
aged D2G	48 ± 11.6	565 ± 135.8	11.8 ± 2.8/nucleus

Table 2.1. Mfn2 levels present in perinuclear space increase as cell numbers decrease with disease. Quantification of Mfn2 protein levels using an unbiased sampling of retina RGCs by immunohistochemistry shows that the amount of Mfn2 found within the perinuclear space is two-fold higher in diseased retina.
**$p < 0.01$, *$p < 0.05$
$n = 3$

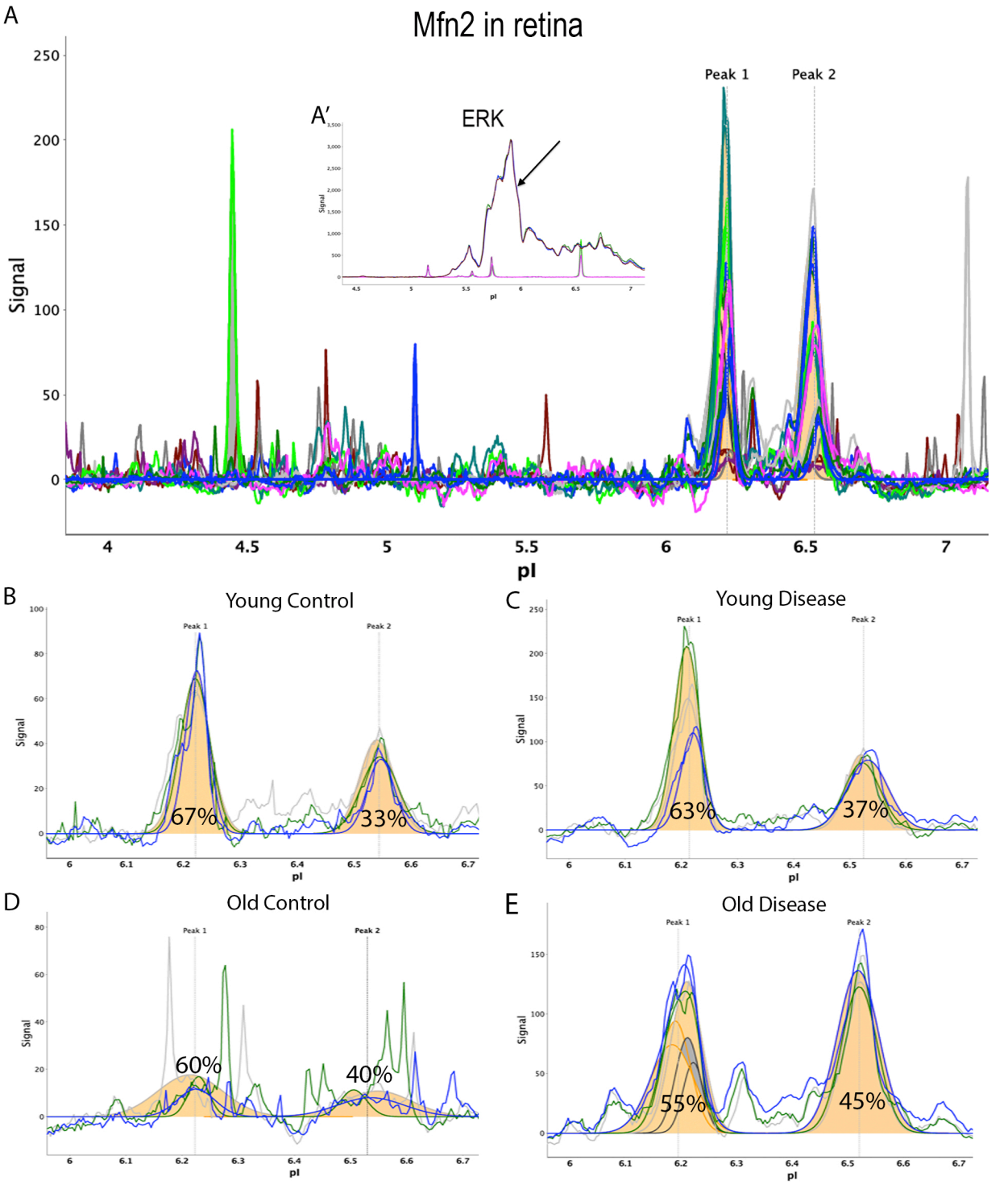

Figure 2.4. NanoPro assay shows differences in protein expression based on age and disease.
A) An overview of multiple tracings shows that there are two specific peaks representing the Mfn2 protein. These peaks occur at the approximate isoelectric points (pI) of 6.2 and 6.5, the latter of which corresponds to the hypothetical isoelectric point (6.52) for Mfn2. The other, randomly occurring spikes prove to be background noise due to lack of replication. A') (inset) The small, lower tracings show ERK levels in HeLa cells, with the upper tracings showing ERK levels in retinal tissue. B-E) Replicate tracings focus in on individual conditions, shown all together in A, further confirming pIs as accurately representing Mfn2. The percentages reflect the average amount of protein in each of the peaks. B) Young control (D2G) retina; C) young disease (DBA) retina; D) aged control retina; E) aged disease retina.

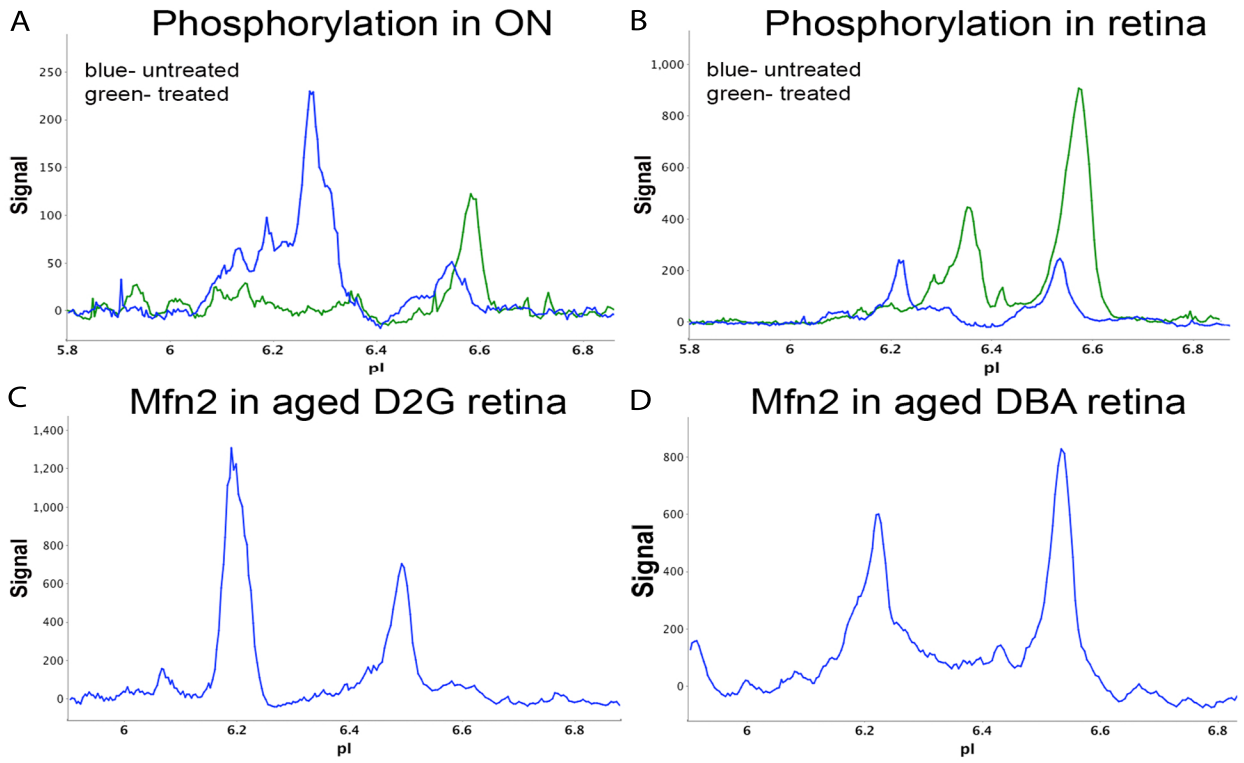

Figure 2.5. Mfn2 displays a selective loss of the phosphorylation-specific peak in diseased animals. A phosphatase-stripping assay performed on the tissues uncovered a near-complete depletion of the 6.2 peak in both tissues (A, B) with a concurrent increase in the second 6.5 peak, indicating that there is an active, phosphorylated isoform of Mfn2 present. This shift to the non-phosphorylated isoform is not due solely to aging (C), but occurs with disease (D). pI- isoelectric point; A,B) blue tracing= untreated tissue, green tracing= tissue treated with lambda phosphatase. Tracings are from one representative animal.

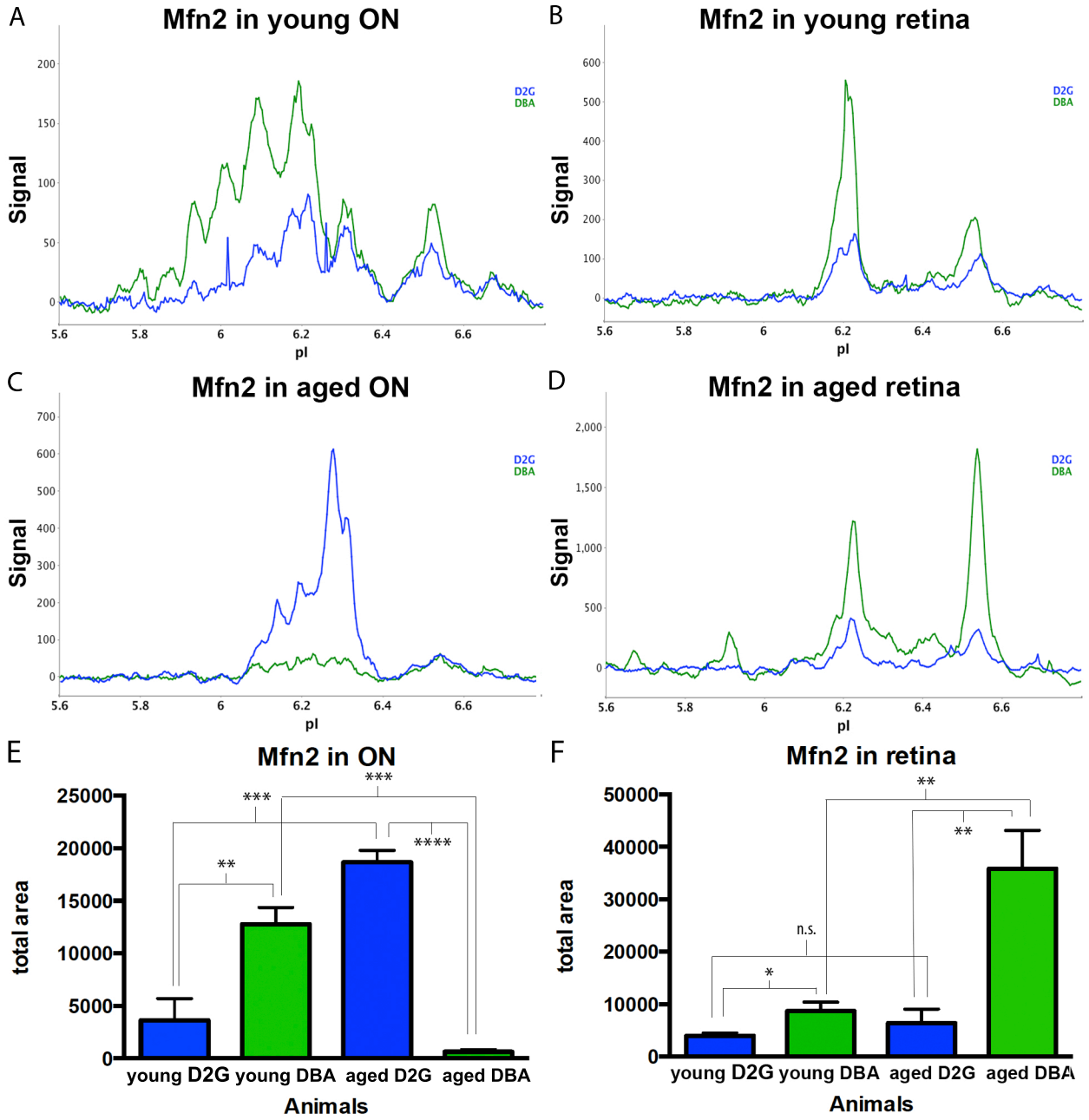

Figure 2.6. Mfn2 protein decreases in diseased ON, while simultaneously increasing in retina with disease. A) In young animals, Mfn2 protein levels are higher in diseased ON tissue. B) In young retina, Mfn2 protein levels are also higher in diseased tissue. C) In older animals, a three-fold decrease in Mfn2 is seen in diseased ON when compared with controls, while D) aged, diseased retinal tissue shows a three-fold increase in Mfn2 when compared to age-matched controls. Another observation is the relative change in peak sizes which correlate with disease progression (B, D). In control animals of both age groups, both Mfn2 peaks are of similar size, indicating the presence of similar amounts of the two Mfn2 isoforms. In young DBA retina, there is a greater amount of phosphorylated Mfn2 present (the 6.2 peak), while there is a shift to an increase in the dephosphorylated Mfn2 isoform (6.5 peak) in the older, diseased retina.

Continued from previous page-
E) Quantification of Mfn2 in ON shows a significant increase in Mfn2 protein in young DBA mice compared to age-matched controls ($p = 0.0036$); an extremely significant increase in Mfn2 in old DBA vs. old D2G ($p < 0.0001$); a significant increase in Mfn2 with age in controls ($p = 0.004$), with a significant decrease in Mfn2 with age in DBAs ($p = 0.002$). F) Quantification of Mfn2 in retina shows a significant increase in protein expression in young DBA mice compared to age-matched controls ($p = 0.0107$); a significant increase in Mfn2 protein in old DBA vs. old D2G retina ($p = 0.0027$); and a significant increase in Mfn2 protein accumulating over time in DBA retina ($p = 0.0033$) which does not occur in D2G retina.
* $p < 0.05$; ** $p < 0.01$; *** $p < 0.001$; **** $p < 0.0001$
pI- isoelectric point; blue tracings= D2G, green tracings= DBA Tracings are from one representative animal; graphs n=3

On following page-
Figure 2.7. Mfn1 levels change similarly in optic nerve of both control and disease animals, while being more variable in retina. A) Mfn1 shows similar expression patterns and levels in both control and disease. The blue and green tracings are in young D2G and DBA, respectively; the pink and burgundy tracings are aged DBA and D2G, respectively. B) While the quantification of total protein levels shows a significant ($p=0.0118$) decrease with aging, there is no difference between control and disease. However, when broken down by individual peak area, there is a major shift from the phosphorylated peak (P1) to the non-phosphorylated peak (P2) that occurs with age ($p = 0.013$).
D-G) In the retina, D) control animals have a significant drop in Mfn1 levels as they age ($p = 0.0034$), while, conversely E) disease animals see a significant increase ($p = 0.0022$). F) In the aged animals, the disease animals express significantly higher levels of Mfn1 ($p = 0.0036$). G) A graphic representation of Mfn1 protein levels in retina in all cohorts reflects the inverse expression pattern between control and DBA animals with age ($p > 0.002$).
D, E) blue tracings = young animals, green tracings = aged animals; F) blue tracing = D2G, green tracing = DBA. pI- isoelectric point; Tracings are from one representative animal; graph n= 3.

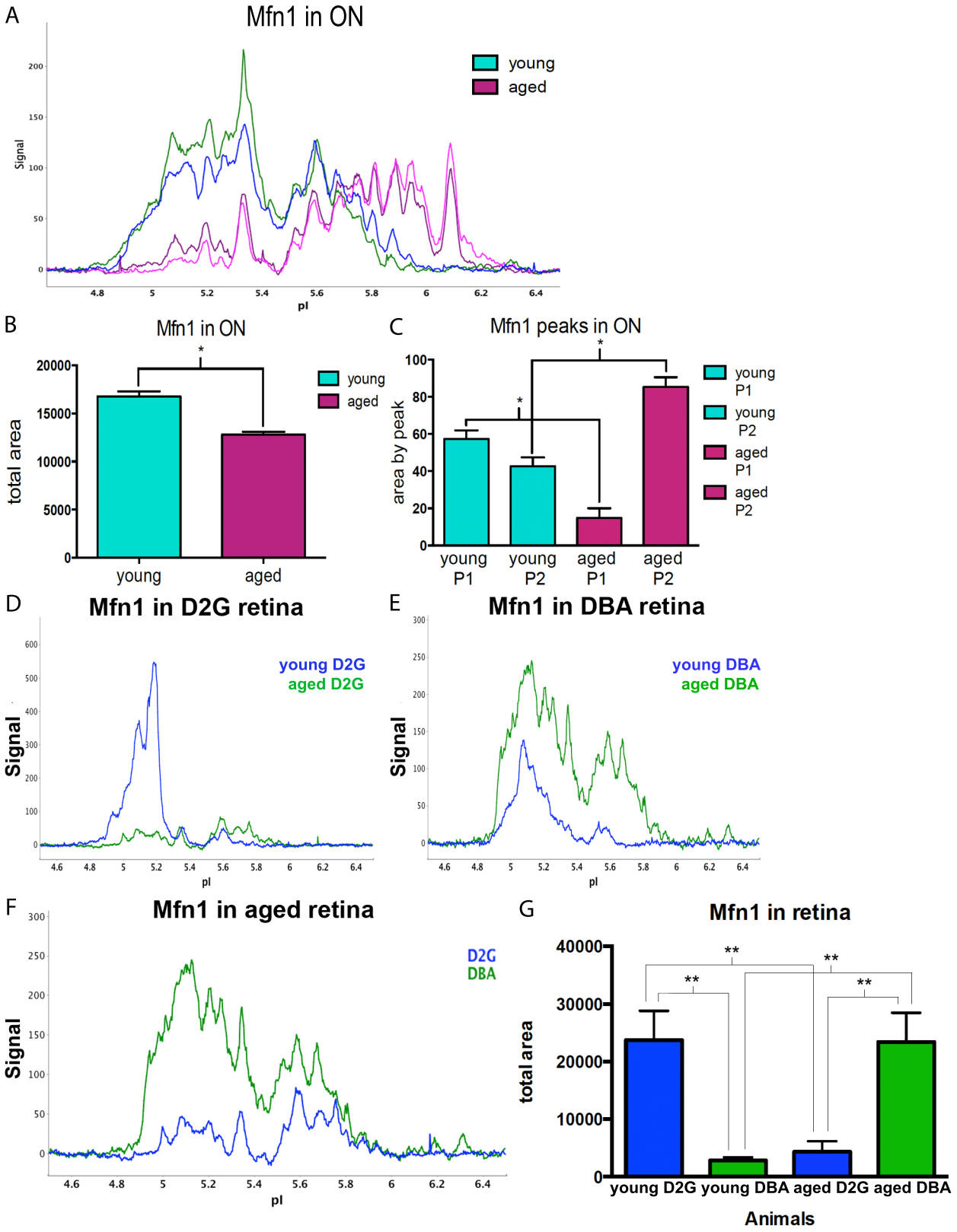
A
Mfn1 in ON
young
aged
Signal
pI
B
Mfn1 in ON
total area
young
aged
C
Mfn1 peaks in ON
area by peak
young P1
young P2
aged P1
aged P2
D
Mfn1 in D2G retina
young D2G
aged D2G
Signal
pI
E
Mfn1 in DBA retina
young DBA
aged DBA
Signal
pI
F
Mfn1 in aged retina
D2G
DBA
Signal
pI
G
Mfn1 in retina
total area
young D2G young DBA aged D2G aged DBA
Animals

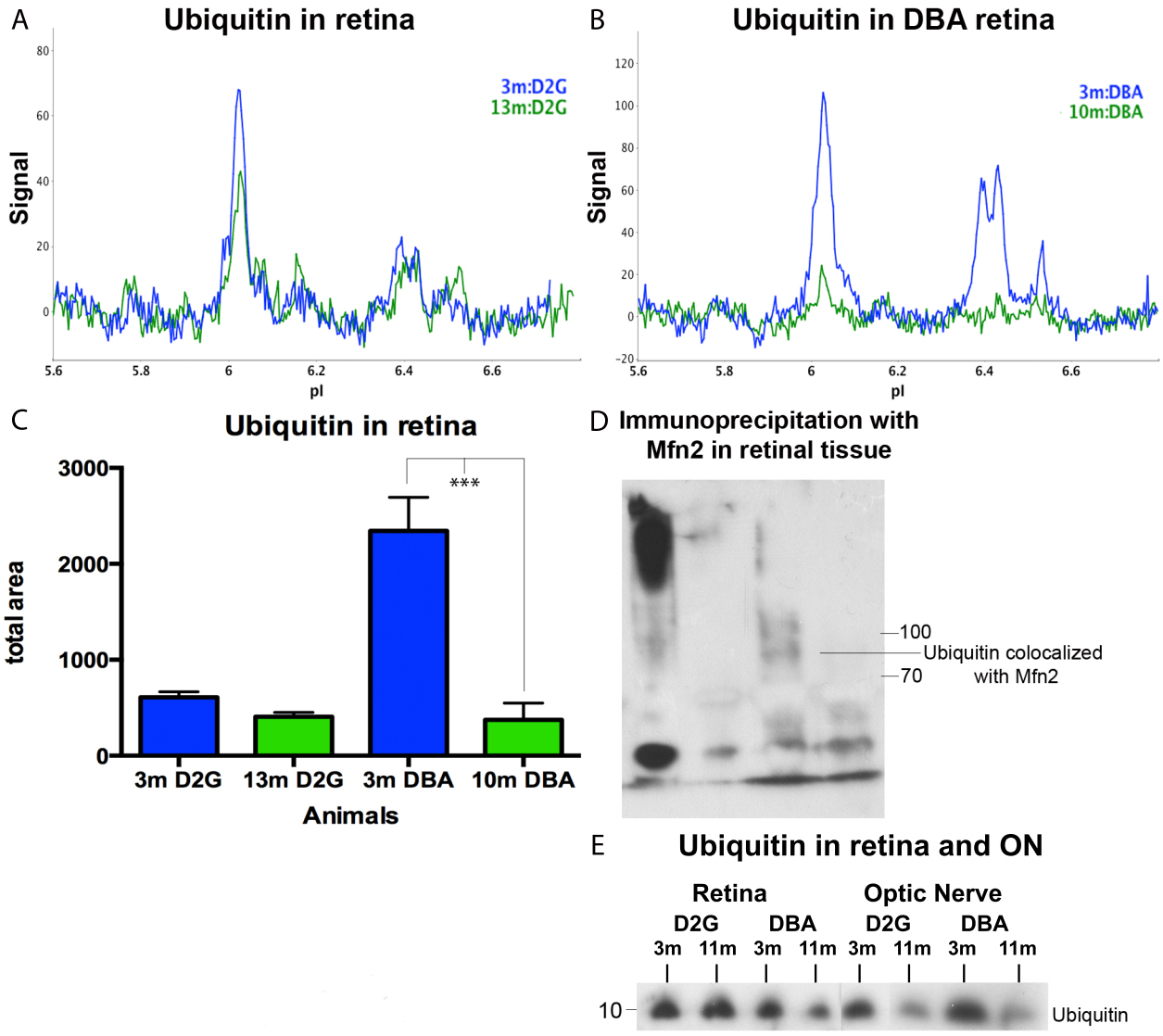

Figure 2.8. Ubiquitin levels are maintained during aging in control retina, while decreasing with disease progression. A) Ubiquitin levels remain stable during aging in control retina, but B) decline significantly ($p = 0.0010$) with disease progression. C) Quantification of ubiquitin expression shows a significantly greater protein expression in 3 month old DBA animals when compared with control animals of any age and with aged DBA animals (*** $p = 0.0010$). When examining ubiquitin levels through Western blot, D) immunoprecipitating with Mfn2 shows ubiquitin colocalizes with Mfn2; and E) ubiquitin levels decrease with disease progression in retina, while remaining steady in control retina, but decrease with age in both D2G and DBA mice in the ON.

Tracings are from one representative animal; graph n=3.

Lane markers in D represent varying urea concentrations applied to tissue during IP: L1 0M, L2 5M, L3 7M, L4 9M.

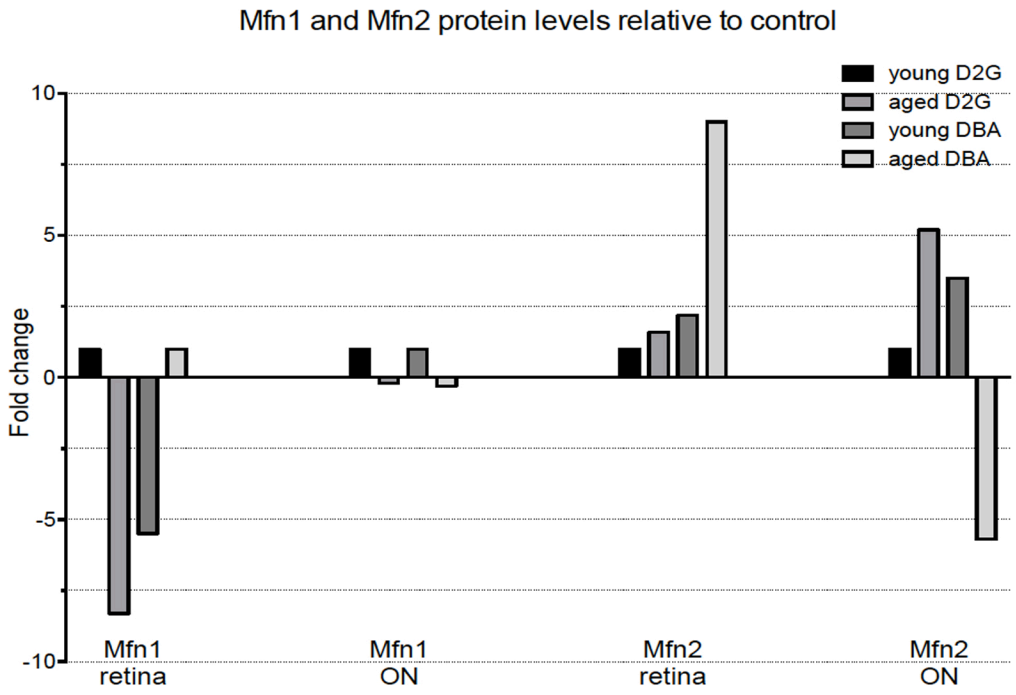

Figure 2.9. Summary of fold change of Mfn1 and Mfn2 protein levels.
Mfn1 in the retina shows a reverse expression pattern between control (D2G) and disease (DBA), with Mfn1 reaching young control levels in aged disease (far left grouping). In optic nerve (2nd grouping from left), there is equal levels and identical expression patterns of Mfn1 protein. In Mfn2, protein levels increase dramatically and statistically in disease (3rd grouping from left), while showing a similar statistically significant decrease in optic nerve. Again, in optic nerve expression pattern is reversed.
All fold changes are in comparison to the young control in each group.

Part III: The presence of increased intraocular pressure causes Mfn2 deficiencies via dephosphorylation separate from the severity of the pressure.

Abstract

Dysfunction of organelle and energy transport along the axolemma are harbingers of all classic neurodegenerative diseases. Previously we described an optic neurodegeneration model where decreased ATP reserve and dysregulation of axonal transport presage axonal loss. Loss of functional connectivity of retinal ganglion cells with the brain occurs in glaucoma and leads to the second most common form of blindness. In this report we investigate the interaction between one of the known risk factors for neural degeneration in glaucoma, intraocular pressure (IOP), with a key regulator of axon energy transport, mitofusin 2 (Mfn2). Mfn2 serves two roles in mitochondrial homeostasis including mitochondrial fusion and transport, the latter being dependent upon its phosphorylation state. Previously, we found that Mfn2 but not Mfn1 accumulates selectively in RGCs during degeneration. In these studies we measure protein levels and phosphorylation state in an in vivo and in vitro model. We demonstrate that Mfn2 is significantly downregulated at 6 months of age. Importantly we show that both mitofusins undergo a select dephosphorylation event that correlates with pressure. Finally, in vitro modeling indicates that pressure induced changes in Mfn2 phosphorylation may be reversible. Together these data indicate that dynamic changes in Mfn2 phosphorylation state should be further studied in order to determine their role in the early loss of energy transport in neurodegenerative diseases.

Introduction

It is well known that elevated IOP is a strong indicator of developing glaucoma (Flanagan, 1998; Friedman DS, 2004; Gordon et al., 2002; Inman et al., 2006) and that it results in loss of RGC axons (Kerrigan-Baumrind et al., 2000). Energetic compromise is reflected by decreased ATP levels in optic nerves (ON) from mice with increased IOP (Baltan et al., 2010; Inman et al., 2013). Increasing evidence indicates that neurodegeneration begins in the axon, with decrease in transport and bioenergetics being factors in the degeneration. With these additional insights being found in glaucoma, it is becoming accepted as a neurodegenerative disease (Calkins and Horner, 2012). Stress-induced mitochondrial dysfunction is found in

neurodegeneration (Celardo et al., 2013; Gonzalez-Cabo and Palau, 2013; Rodriguez-Martinez et al., 2013). IOP induces stress in glaucoma.

Mitochondrial transport has previously been shown to be disrupted in neurodegenerative disease (Celardo et al., 2013; Crish et al., 2013; Gonzalez-Cabo and Palau, 2013; Rodriguez-Martinez et al., 2013), and specifically in glaucoma (Crish et al., 2013) (Inman, data in progress). Transport disruption has been shown tied to the dysfunction of Mfn2 in dorsal root ganglion cells (Misko et al., 2010). Taken together, we hypothesized that dysfunction of Mfn2 contributes to transport dysfunction in neurodegenerative disease. Glaucoma, with its long axonal projections from retina to the brain, is a well-characterized disease in which to examine axonal transport loss.

Mitochondria are critical to meet the high bioenergetic demands of a neuron; this is achieved by maintaining a balance between mitochondrial biogenesis, mitochondrial trafficking, and mitochondrial dynamics. The mitofusin proteins Mfn1 and Mfn2 are critical in all three of these areas (Misko et al., 2010; Rodriguez-Martinez et al., 2013). Previous findings by our lab and others, indicate Mfn2 dysregulation compromises the mitochondria's ability to function properly. Recently, our laboratory has shown that the mitofusins, particularly Mfn2, play a contributory role in disease progression as well (Chapter 2). The discovery of an active phosphorylated state of Mfn2 in retina and optic nerve has led to exploration of the role of IOP on the post-translational modifications of Mfn2 in glaucoma.

To better understand the role of IOP in glaucomatous loss of vision, it is important to determine empirically how departures from normal IOP and chronic elevations in IOP correlate with pathologic changes in the optic nerve. We used both *in vivo* and *in vitro* models to examine post-translational modification of Mfn1 and Mfn2. Here, we show that it is not the severity of IOP, but rather the length of time with the disease manifested, that causes the neurodegeneration in the RGCs. We further show that the removal of pressure from RGCs allows mitochondria a chance to recover, and thus likely allow the cells to function at a higher level for a longer time.

Methods

Animals

Experiments were conducted in accordance with regulations set forth in the Association for Research in Vision and Ophthalmology Statement for the Use of Animals in Ophthalmic and

Vision Research, and were conducted under protocols approved by the Institutional Animal Care and Use Committees at the University of Washington (UW). DBA/2J (DBA/diseased) mice and DBA/2JGpnmb+ (D2G/control) were initially obtained from Jackson Laboratories (Bar Harbor, ME), and bred and maintained at a pathogen-free facility in the UW vivarium at the South Lake Union facility, with new breeding pairs incorporated into the colony every year (Inman et al., 2006). All animals were kept on a 12-hour light/dark schedule with ad libitum access to food and water. Mice were three to thirteen months old at the time of tissue collection.

DBA/2J (DBA) mice are a well-established mouse model of glaucoma (Howell et al., 2007; John et al., 1998; Libby et al., 2005; Rangarajan et al., 2011). These mice have spontaneously developed two mutations (Anderson et al., 2002; Chang et al., 1999) resulting in the development of elevated IOP and glaucoma as they age, in a similar fashion as humans. The DBA/2J^{Gpnmb+} (D2G) mice are genetically identical, except they have only one of the two mutations, and do not develop glaucoma, thus act as the control for both disease and aging studies.

Age-matched animals were used in all experiments. Young animals were 3 months old; 6 month animals were 5-7 months; aged animals were 9-10 months.

Pregnant Sprague-Dawley rats were obtained from Charles River at TPE 14, and housed at UW under protocols approved by IACUC on a 12-hour light/dark schedule with ad libitum access to food and water. Pups were P1-2 at the time of primary RGC collection.

IOP analysis

Intraocular pressure was measured as previously described (Inman et al., 2006). Briefly, IOP was taken in lightly anesthetized (Avertin, 1.3% tribromoethanol, 0.8% tert-amyl alcohol) mice using the TonoLab rebound tonometer from ICare, calibrated for mice. Ten tonometer measurements were taken and recorded on each eye. Measurements were averaged together to determine final IOP. We measured IOP in the mice every other week for two months prior to harvesting, to gauge disease progression in the DBA and control conditions in the D2G.

Tissue preparation

Animals were anesthetized with Beuthanasia and the eyes were removed with the optic nerve still connected. The retina was removed from the orb, and the optic nerve was snipped free

of the back of the eye. The brain was exposed in the skull and the superior colliculus region was excised. The tissues were collected, and snap frozen for future protein or RNA analysis as described below. Tissue collected for protein analysis was placed into tubes on dry ice, weighed, and ice-cold lysis buffer was added in a weight-to-volume ratio of 5-10 ml lysis buffer per mg of tissue.

Protein sample analysis

Retina, optic nerve and superior colliculus were removed from mice that had been lethally anesthetized with Beuthanasia. Tissue samples were immediately placed into tubes being stored on dry ice. Tubes were weighed prior to and after the addition of the tissues to determine tissue weight, and maintained on dry ice. For every mg of tissue, 5-10 ml of ice-cold Bicine/CHAPS lysis buffer (with protease inhibitors and DMSO freshly added) was added to the tube. Tissue was broken down using a hand held homogenizer (Kontes Pellet Pestle Motor) to homogenize the mixture and spun to remove cellular debris. The supernatant was placed to a fresh, chilled microcentrifuge tube. Lysate concentration was determined using BCA assay (Pierce). Lysates were frozen and stored at -20 °C until used.

For use in nanoimmunoassays (O'Neill et al., 2006), lysates were diluted to a final concentration of either 0.05 mg/ml (retina, superior colliculus (SC)) or 0.1 mg/ml (ON) using SERVALYT^{TM} 4-7 carrier ampholyte and resolved by capillary isoelectric focusing electrophoresis using the NanoPro 1000 (ProteinSimple) according to our developed protocols (Nivison, ProteinSimple Application Briefs #1032, #1033, 2012). Resolved proteins were immobilized using UV crosslinking, then probed with primary antibodies in the following concentrations: α-Mfn1 (rabbit, 1:300, Santa Cruz), α-Mfn2 (rabbit, 1:25, Sigma); α-Ubiquitin (rabbit, 1:50, Cell Signaling). Secondary antibodies (ProteinSimple) used include: goat α-rabbit biotin conjugate (1:100) and streptavidin-HRP (1:100). Luminol/Peroxide XDR was used for signal detection. All traces and calculations of peak areas were performed using Compass 1.8.1 (ProteinSimple).

Cell separation and culturing

Primary cell separation was performed using the protocol previously developed in the Calkins laboratory (Sappington et al., 2006). Briefly, primary cultures of retinal ganglion cells

were derived from P1-P2 Sprague-Dawley rats, with 7 animals per collected group. Retinas were dissociated by trituration and papain, DNase 1 in EBSS (Earle's balanced salt solution). Viability was assessed by trypan blue exclusion. The ganglion cell populations were then purified using magnetic beads (MACS Miltenyi Biotec) to tag the chosen cell type and magnetic columns (MACS Miltenyi Biotec) for separation, then cultured in a growth medium. Cultures were allowed to grow in chamber slides for approximately 4 days prior to placing chambers under pressure, replacing 100% of the medium 12 hours after plating, then changing the medium every 48 hours. A final medium change occurred prior to the onset of the experiment.

Each group of harvested cells was evenly split between two chambers, with one chamber remaining at ambient pressure and the other undergoing increased pressure for 24 or 72 hours.

Cell harvesting

Using a modified cell harvesting protocol from ProteinSimple, the cells were washed with a low-salt cell wash prior to briefly incubating in Trypsin/EDTA. Trypsin was then inhibited with 10% FBS in medium. Upon further washes, the cells were removed with a scraper, and collected into labeled tubes. An additional rinse of the chamber allowed for the collection of all remaining cells. Cells were spun down and the supernatant discarded. Bicene/chaps with DMSO and protein inhibitors was added to the remaining pellet per the protocol table (10-20 uL). The pellet was then broken up in the bicene/chaps and vortexed. The resultant lysate sat on ice prior to spinning down again. The supernatant was then saved in fresh, labeled tubes.

Cell wash, bicene/chaps and DMSO with inhibitors were all from ProteinSimple and specifically designed to work with the NanoPro.

Hydrostatic pressure experiments

Neuronal cultures were exposed to either ambient or +70-mm Hg pressure for 24 and 72 hours as previously described. Pressure exposure occurred in a humidified pressure chamber equipped with a regulator and gauge. The entire chamber was placed in a 37°C incubator, with an air mixture of 95% air and 5% CO2 pumped into the chamber to create the pressure. Cells under ambient pressure were maintained in a standard incubator at 37°C (Sappington et al., 2006).

Cells were harvested at timepoints 24 hours and 72 hours, after exposure to either ambient pressure or high pressure. An additional group was kept under high pressure for 72 hours and then allowed to remain an additional 24 hours at ambient pressure prior to harvesting. For all cultures, 100% of the media was replaced immediately before experimentation.

Statistical analysis

All data in this study are expressed as the mean ± SEM, except where otherwise indicated. Correlation coefficients, corresponding p values, and outliers were calculated using GraphPad Prism 3.0 (GraphPad Software, San Diego, CA) and Prism 6.0. Groups were compared using ANOVA with Welch's correction assuming a nonparametric comparison, ANOVA, two-way ANOVA, and unpaired t-tests.

Results

Knowing that IOP frequently contributes to glaucoma's progression, we looked further at the post-translational modification of Mfn2 to unveil any correlation between them. To test this hypothesis, it was necessary to focus more closely at both the 9 month time point, when disease is present and mice are already blind, and the 6 month time point, when the disease begins to outwardly manifest itself and IOP begins to rise. The expectation was to see a correlation between the severity of IOP and the noted changes in Mfn2- a steady increase in Mfn2 in the retina, and a steady decrease in Mfn2 in the optic nerve.

IOP variability does not alter mitofusin levels in retina or ON at 9 months

In contrast to expectations, what was observed was that variable IOPs do not cause significant changes in mitochondrial fusion proteins at 9 months in retina or ON (Figure 3.1a-c). In retina, there is a significant change in levels of Mfn2 between disease and control (Figure 3.1c), but IOP is not correlated to Mfn2 expression (Figure 3.1a, 3.1b). Instead, individual variability of IOP results in similar levels of Mfn2. In diseased animals, IOPs ranged from 12.6 to 24.4 and showed animal-to-animal variability rather than IOP correlation.

In optic nerve, there is a significant difference in Mfn2 levels between control animals and diseased animals as well (Figure 3.1f), but no difference between the various IOPs (Figure 3.1d, 3.1e). Again, IOP does not correlate to Mfn2 expression levels.

In evaluating Mfn1 or ubiquitin levels in relation to IOP at 9 months, no significant changes are noted in retina or ON (data not shown). Changes in Mfn2 and ubiquitin, but not Mfn1, were observed in SC at 9 months that appeared to correlate to IOP.

IOP increase corresponds to changes in Mfn2 at 6 months

After determining that IOP does not correlate with levels of Mfn1 or Mfn2 at 9 months, the hypothesis was that this negative result may have been influenced by pathology of the axon at this more chronic period. The focus shifted to examine more closely the 6 month timepoint when the disease has initiated and is progressing. At 6 months, the early disease phase, an increase in IOP causes a corresponding increase in Mfn2 levels in the retina and ON, but causes no significant changes in SC. Examining the NP tracings at 6 months shows the similarity of Mfn2 levels in control retina across varying IOPs (Figure 3.2a), while showing a spike in Mfn2 levels in the DBA when the IOP increases (Figure 3.2b). Comparing 6 month cohorts, there is a significant drop in Mfn2 occurring in DBA ON ($p = 0.0047$). While the controls show no significant difference between 6 and 9 months, the decrease in Mfn2 is even more significant by 9 months ($p < 0.0001$).

Mfn1 begins to change expression in retina and ON as well at 6 months, expressing similar levels in controls and DBAs having similar IOPs. Overall, Mfn1 trends downward in 6 month controls and DBAs with increasing IOP, until the IOP jumps to a definite disease level (18.1) (data not shown). Ubiquitin also changes levels in the ON. There is a spike in ubiquitin at 6 months, with it dropping back to control levels by 9 months (data not shown).

To further evaluate the effect of IOP versus the length of time with the disease manifested, we examined D2G animals, 6 and 9 month DBAs all having the same IOP. There is a significant decrease in overall Mfn2 levels in retina when comparing control and DBA, with a further decrease by 9 months (Figure 3.2e). Interestingly, the change in overall Mfn2 is most strongly reflected in the loss of the phosphorylated peak (Figure 3.2f) occurring at 6 months, with all peaks decreasing by 9 months.

When examining the same IOP in the optic nerve, Mfn2 levels dropped significantly with extended exposure to pressure, which led to the conclusion that it was the length of time of disease manifestation, not the severity of IOP, that causes the change. Thus, elevated IOP becomes a significant indicator of disease at 6 months.

Dephosphorylation of Mfn1 and Mfn2 occurs early in disease

After exploring the expression level of Mfn2, we quantitatively measured the two states of Mfn2 previously described (Chapter 2). Mfn2 has an active phosphorylation peak whose size changes in relation to the non-phosphorylated peak. An overview of the 9 month data indicate a shift from the phosphorylated state to the non-phophorylated state in DBA mice when compared with controls (see Figure 3.1a, 3.1d). While the controls of both ages tend to run with a 60/40 ratio (average) of phosphorylated to non-phosphorylated, that shifts to the opposite ratio of 40/60 (average) in the older diseased animals, with variability again not specifically related to IOP.

However, looking to the earlier timepoint of 6 months, both Mfn1 & Mfn2 states shift from phosphorylated to dephosphorylated early in disease. The tracings from the NP consistently reveal a shift from the more phosphorylated state to the non-phosphorylated state (figures 3.2a, 3.2b, 3.2e, 3.2f). In retina, there is a shift from a 60% phosphorylated Mfn2 state in control (Figure 3.3a) to 40% non-phosporylated Mfn2 state in disease (Figure 3.3b) begins as early as 6 months. An even more pronounced shift in Mfn1 begins at 6 months in the SC, with 70% of Mfn1 in a more phosphorylated state (Figure 3.3c) in controls, decreasing to only 45% in age-matched disease (Figure 3.3d). This shift seen in the SC is even more dramatic when appreciating that the total amount of protein is equal and IOPs are the same.

Pressure dynamically regulates Mfn2 and ubiquitin levels, but not that of Mfn1, after 72 hours

To further explore what role IOP plays in the changing Mfn2 levels, we cultured rat RGCs and put them under pressure for varying lengths of time (Sappington et al., 2006). This allowed the focus to be on the sensitivity of only the ganglion cells to pressure. Each batch of cells was split between two chambers on separate slides, where approximately 50,000 cells per chamber were plated. One half (one chamber) of each batch remained at ambient pressure, while the other half was placed under elevated pressure. Pressure elicited changes in Mfn2 and ubiquitin protein levels, but not Mfn1, after 72 hours. Tracings from NP show the difference in levels of Mfn2 (Figure 3.4a) and ubiquitin (Figure 3.4b) after 72 hours of pressure, with Mfn2 levels increasing and ubiquitin levels decreasing. Quantification of the amount of protein shows changes in Mfn2 levels approaching significance ($p=0.0594$) after applying pressure for 72 hours

(Figure 3.4c), while ubiquitin levels drop quite significantly ($p=0.0034$) under the same conditions (Figure 3.4d).

Once it was determined that pressure did affect changes at 72 hours, we looked at 24 hours to see whether the changes are induced earlier. Changes in Mfn2 and ubiquitin begin as early as 24 hours after pressure is applied on RGCs *in vitro*. NP traces evaluating the changes after 24 hours of pressure show little difference in Mfn2 expression levels at ambient pressure (Figure 3.4e, 3.4f), but with small changes evident. Upon quantification (Figure 3.4g), the change in Mfn2 is trending upward even at the earlier timepoint, highlighting that changes to Mfn2 protein expression begins with a very early onset of pressure.

Mfn2 phosphorylation state returns to control levels when pressure is removed *in vitro*

Because the changes to Mfn2 begin shortly after pressure is induced, we wanted to determine whether cellular recovery could occur if intervention was initiated after the changes had activated. Thus, we chose to examine the effects of transient pressure on RGCs. We again split each cell group between two chambers and put two-thirds of the chambers under pressure for 72 hours, and left one-third at ambient pressure. After 72 hours, all the chambers were removed from pressure. One half of the pressured cells were placed at ambient pressure for an additional 24 hours prior to harvesting, while the other set of cells was harvested immediately, as were the chambers of cells left at ambient pressure for 72 hours.

In visualizing the cells, we found that, in ambient conditions, the cells maintained their processes throughout the time elapsed (Figure 3.5a). Those cells subjected to 72 hours of pressure had lost their processes, and many appeared fractured (not shown). The cells that were allowed time to recover for 24 hours before harvesting appeared less stressed, though they had not re-extended any processes (Figure 3.5b).

Upon measuring Mfn2 levels in the ambient cells, the 72 hour constant pressure, and 72 hours of pressure followed by 24 hours of recovery at ambient pressure, we found a decrease in Mfn2 levels in the 72 hour pressure cells, with a return of the Mfn2 levels to the ambient Mfn2 levels in the cells subjected to pressure but allowed time to recover (Figure 3.5c). When quantifying the total Mfn2 protein, the data suggest that there was a rescue of much of the protein when the RGCs were allowed to recover (Figure 3.5d). Importantly, the recovery was in

the phosphorylated state of Mfn2 (dark portion of bar in 3.5d). These data warrant further group testing to confirm the statistical relevance of this exciting observation.

Discussion

Increasing evidence indicates that neurodegeneration begins in the axon and its terminals, with decrease in transport and bioenergetics being the potentially key tipping point. The mitofusins are regarded as key regulators of mitochondrial biogenesis and mobility. Mutations in mitochondrial fusion proteins lead to human neurodegenerative diseases such as optic atrophy type 1 and Charcot-Marie-Tooth II. In our previous work we showed that mitochondrial mutation frequency does not increase further with age or raised IOP in glaucoma. Nevertheless, we discovered that an active phosphorylated state of Mfn2 in retina and optic nerve undergoes significant changes in post-translational modification and distribution in glaucoma.

It has been shown by others that there are events occurring even earlier in the disease (Baltan et al., 2010; Bosco et al., 2011; Howell et al., 2007). In the mouse model of glaucoma presently studied, manifestation of the disease normally begins at around 6 months of age. Turning the focus to that time frame, we continued to look at modifications to the mitofusins. Because of our earlier discovery of the phosphorylation changes in Mfn2, we again focused on those changes closer to disease onset.

Using the diseased state as a starting point for analysis of mitochondrial changes, we found that severity of IOP does not contribute any additional modifications of levels of dysfunction of the mitofusins. Instead, we found that, once disease is present, it is the length of time that pressure is imposed that then contributes to disruption, and likely the furtherance of neurodegeneration in the RGCs. This implies that it is earlier in the disease that the changes begin, and where treatment could most efficaciously be targeted.

A major finding was the shift in protein from a more phosphorylated state to the non-phosphorylated state occurring at this earlier stage. While this shift was evident at 9 months, we were able to show that, as IOP increased enough to trigger the disease, there was a corresponding shift of the state to the non-phosphorylated without changes to overall protein levels at the earlier time. Because of the role of Mfn2 in transport, it is likely that this state change, from phosphorylated to dephosphorylated, plays a role in disrupting mitochondrial transport, as well

as dysregulating the supply of necessary energy to meet the demands of a stressed cell (Celardo et al., 2013; Misko et al., 2010).

Phosphorylation of Mfn2 is modified by pressure and it is reversible. It appears, that while recovery may not be complete in such a short time at the cellular level, we demonstrate that the removal of pressure from RGCs allows the cells to begin to recuperate and their mitochondria have a chance to return Mfn2 to its phosphorylated state. The reestablishment of the phosphorylated Mfn2 reflects early recovery of the mitochondria, and thus likely allow the cells to function at a higher level for a longer time. A longer recovery period may have also exposed further cellular recovery in the regrowth of axonal processes. While these findings may only support the slowing of disease progression, rather than a permanent reversal, maintaining the health of the RGCs as long as possible is a viable endpoint for treatment.

These data indicate that phosphorylation is dynamically regulated by pressure on the order of hours or days. A proposed model for the dephosphorylation of Mfn2 may be tied to kinase activity. The early, but reversible, effect of pressure may be induced by the suppression of kinases active in the cell. In glaucoma, increasing IOP places stress on the cells, which may then act to suppress the kinases. Because some kinases act quickly, while others act more slowly, removal of the pressure (stress) may prevent the suppression of the slower acting kinases. This hypothesis needs further exploration to uncover which kinases are present and deactivated, or oppositely, which phosphatases may be triggered by IOP to become active.

These data argue for further exploration of the relationship between pressure and the phosphorylation state of Mfn2. These data may have implications for how to interpret the mechanisms of pressure lowering drugs. Further research is needed to determine *in vivo* if dynamic regulation of Mfn2 phosphorylation occurs and if this correlates with axonal transplant and energy. Future research may discover whether pressure-lowering drugs mediate their neuroprotective effects through indirect facilitation of axonal transport and maintenance of a normal Mfn2 phosphorylation state.

Our examination of Mfn2 in the context of glaucoma has significance for other neurodegenerative diseases as well. There is evidence among many neurodegenerative diseases that disease-specific stress causes disruption of healthy mitochondrial bioenergetics (Celardo et al., 2013; Gonzalez-Cabo and Palau, 2013; Rodriguez-Martinez et al., 2013). As the effect of

Mfn2 phosphorylation and dephosphorylation appears to be a stress response in neurons, this connection should be further explored in other diseases.

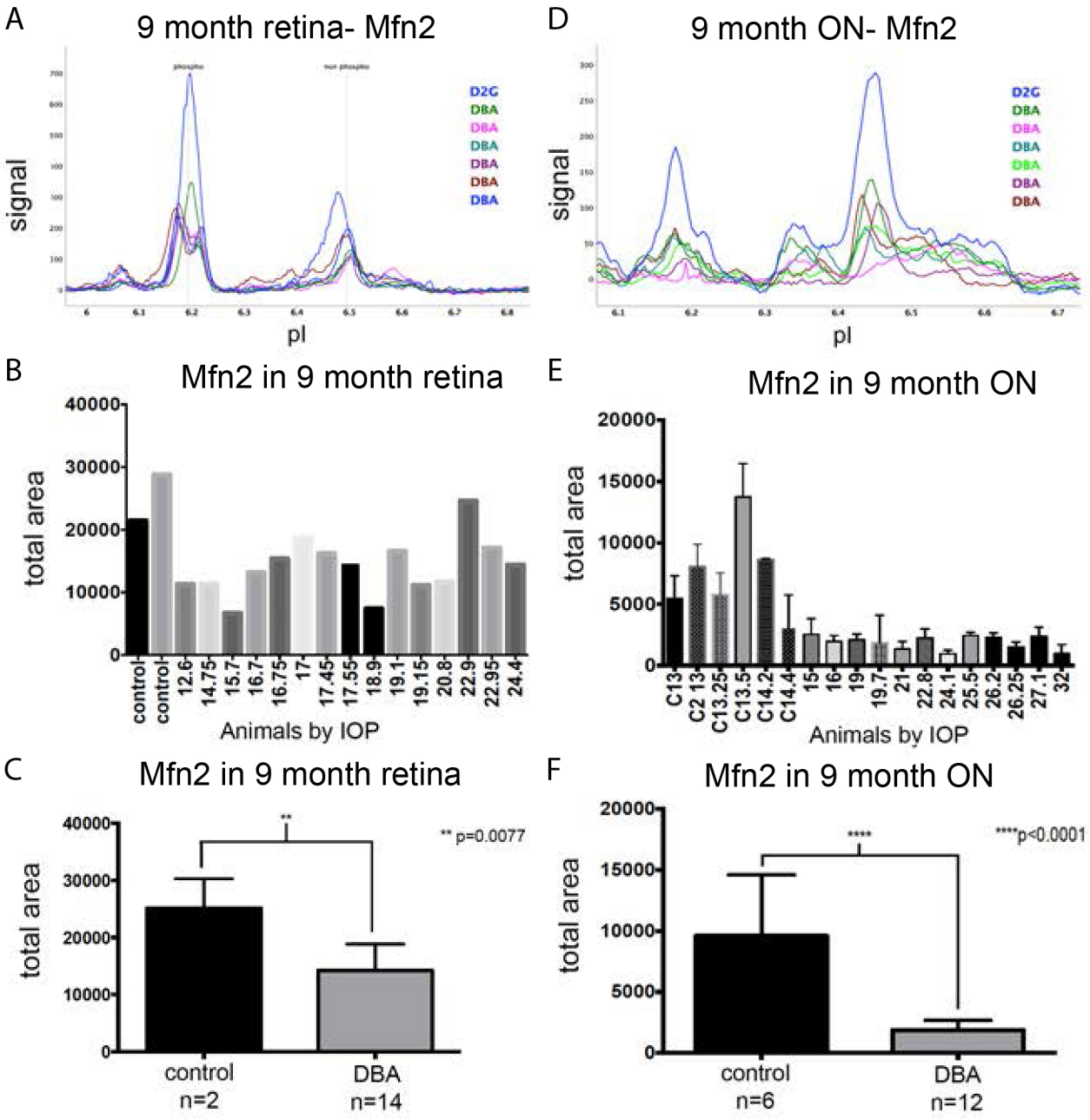

Figure 3.1. IOP variability causes no significant changes in mitochondrial fusion proteins at 9 months in retina or ON.

A-C. In retina, Mfn2 levels do not change due to variability in IOPs. There is a significant change between disease and control (C), but IOP alone is not the cause (A, B).

D-F. In optic nerve, there is a significant difference in Mfn2 levels between control animals and diseased animals (F), but no difference between the various IOPs (D, E).

A & D show NP tracings reflecting the similarity of Mfn2 expression in diseased retina and ON; the tallest peaks are controls, the other six tracings have IOPs ranging from 12.6 to 24.4. B & E reflect the individual variability of IOPs and Mfn2 levels in both cohorts (disease and control), while C & F compare cohorts irrespective of IOP.

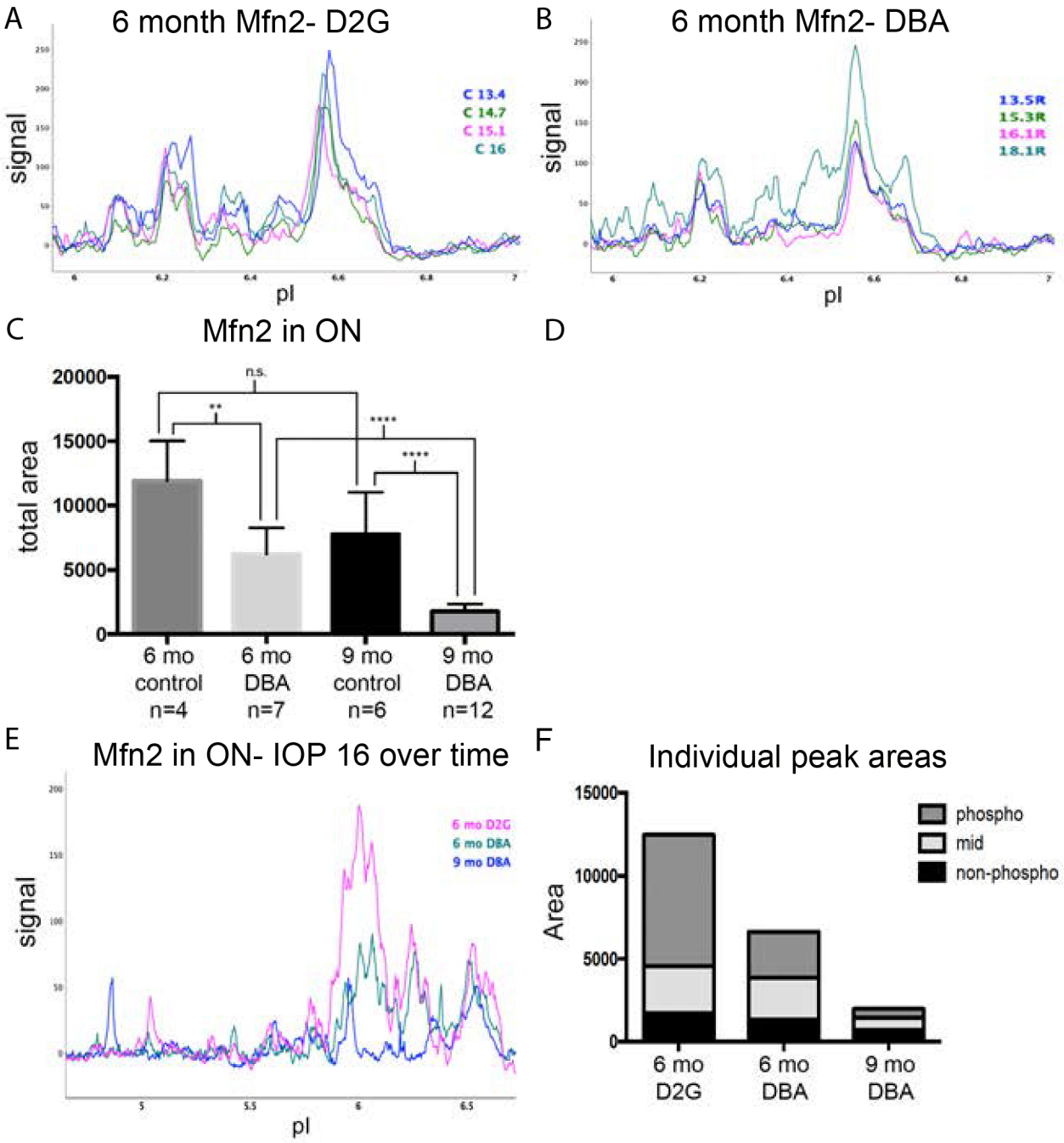

Figure 3.2. Increase in IOP correlates with Mfn2 changes at 6 months in retina and ON. Examining the NP tracings at 6 months shows the similarity of Mfn2 levels in control retina across varying IOPs (A), while showing a spike in Mfn2 levels in DBAs when the IOP increases (B). C) Comparing 6 month cohorts, we see a significant drop in Mfn2 occurring in DBA ON ($p=0.0047$). While the controls show no significant difference between 6 and 9 months, the decrease in Mfn2 is even more significant by 9 months ($p<0.0001$). E) Evaluating Mfn2 levels in animals with the same IOP (16), we find there is a significant decrease in overall levels when comparing control and DBA, with a further decrease by 9 months. Interestingly, the change in overall Mfn2 is most strongly reflected in the loss of the phosphorylated peak (F) occurring at 6 months, with all peaks decreasing by 9 months.

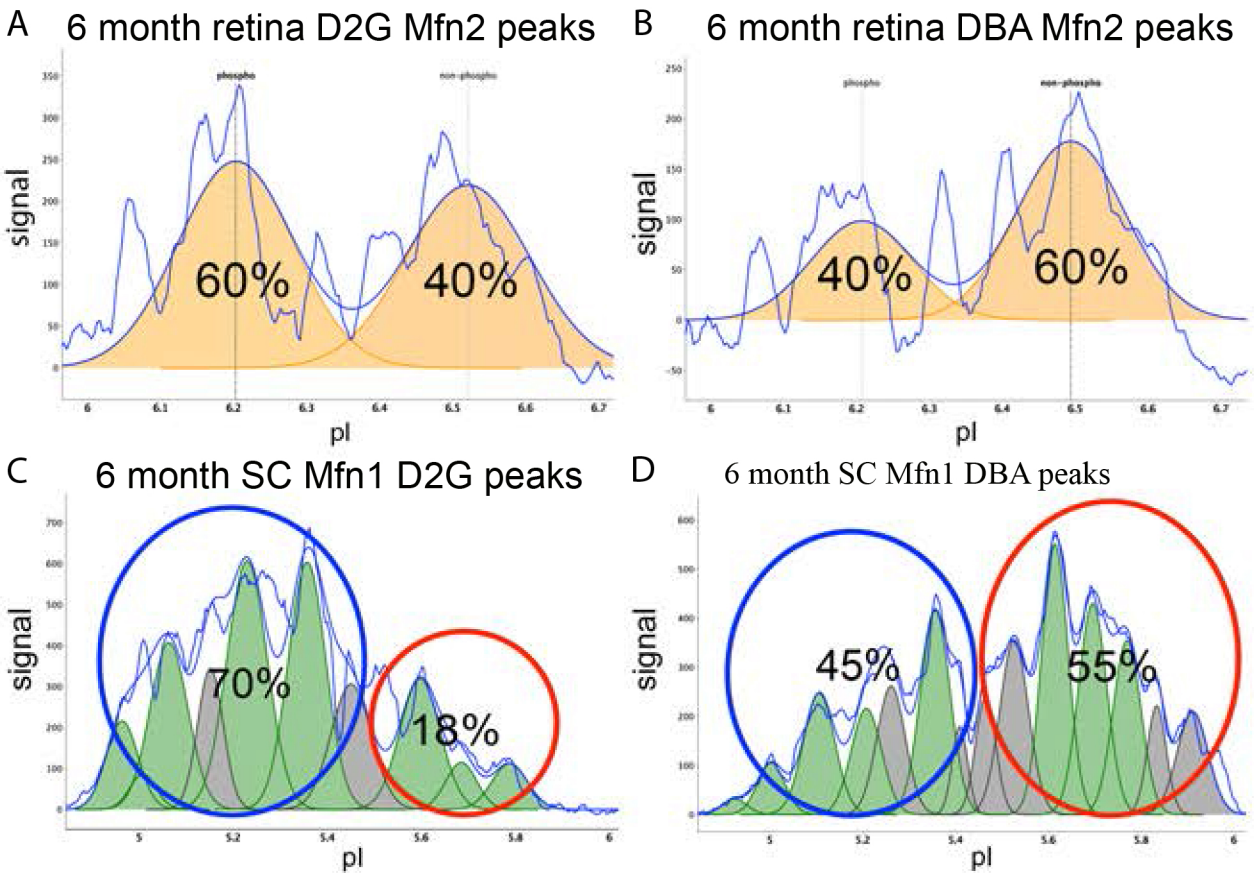

Figure 3.3. Mfn isoforms shift from phosphorylated to non-phosphorylated in both mitofusins early in disease.

Representative tracings from the NP reveal a shift from the more phosphorylated state to a less phosphorylated state. A, B) In retina, we see a shift from a 60% phosphorylated Mfn2 isoform in control (A) to 40% non-phosporylated Mfn2 isoform in disease (B) begins as early as 6 months. C, D) An even more pronounced shift in Mfn1 begins at 6 months in the SC, with 70% of Mfn1 in a more phosphorylated state (C) in controls, decreasing to only 45% in age-matched disease.

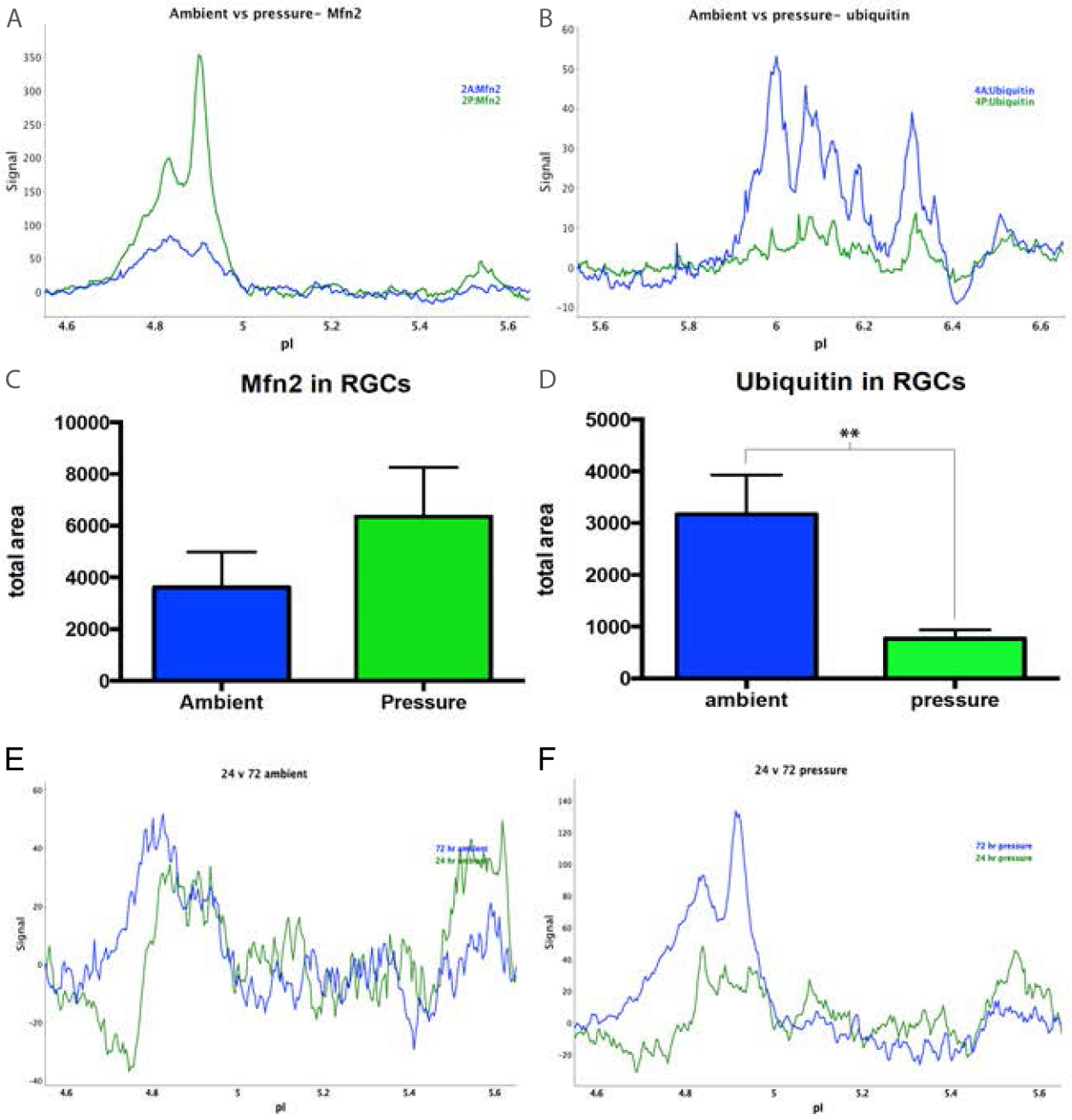

Figure 3.4. Changes in Mfn2 and ubiquitin begin as early as 24 hours after pressure is applied on RGCs in vitro. A, B) Tracings from NP showing the difference in levels of Mfn2 (A) and ubiquitin (B) after 72 hours of pressure. C, D) Quantification of the amount of protein shows changes in Mfn2 levels approaching significance (p=0.0594) after applying pressure for 72 hours, while ubiquitin levels drop quite significantly (p=0.0034) under the same conditions. NP traces (E, F) evaluating the changes after 24 hours of pressure show little difference in Mfn2 expression levels at ambient pressure (E), but small changes beginning under pressure. Upon quantification (G), the change in Mfn2 is trending upward even at the earlier timepoint.

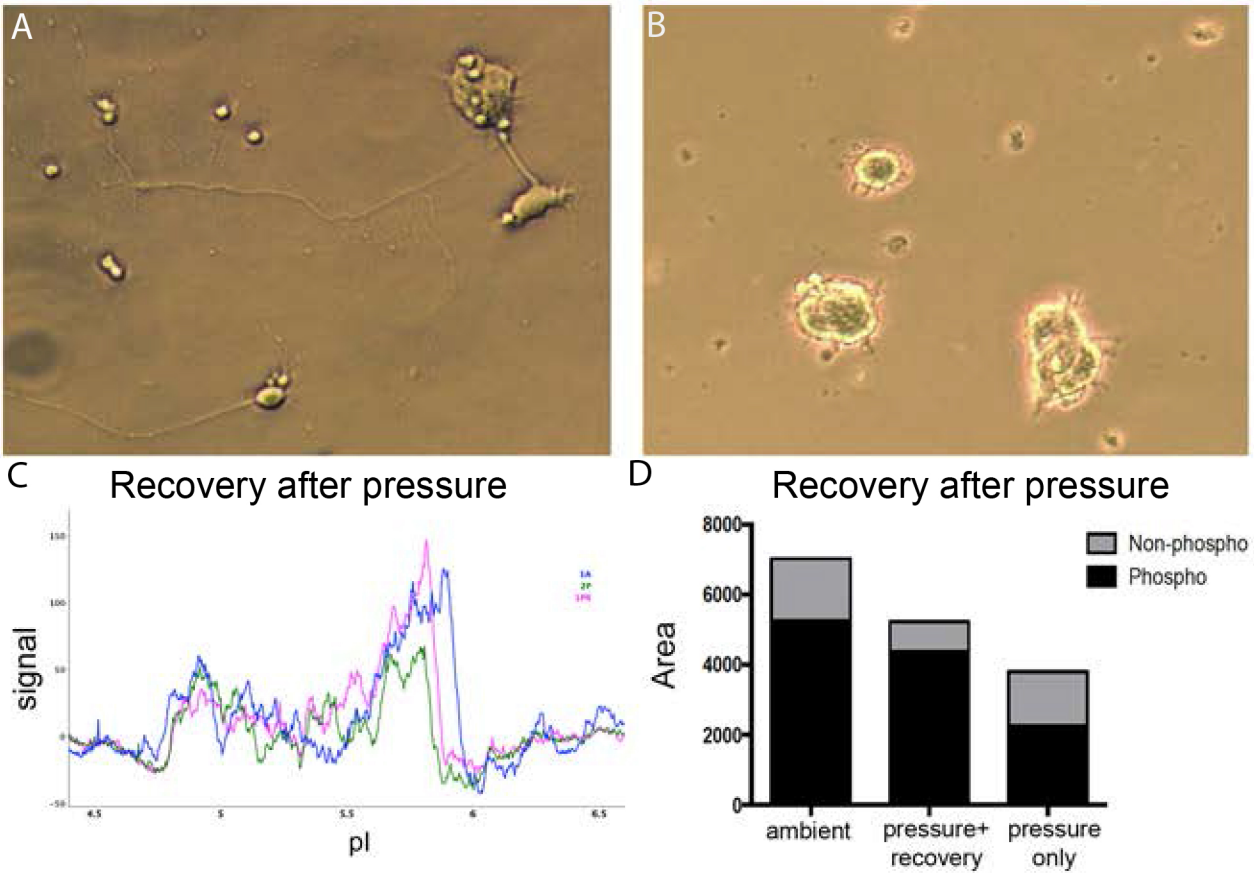

Figure 3.5. Cells in vitro begin to recover after pressure is removed.
A, B) RGCs at 20x magnification. A) RGCs after 72 hours in ambient pressure show processes extending from cell to cell. B) RGCs after 72 hours of pressure, then 24 hours of recovery in ambient pressure show stressed cells with no processes.
C) NP tracing of Mfn2 levels under ambient conditions (blue), 72 hours of pressure (green), and 72 hours of pressure followed by a 24 hour recovery at ambient pressure (pink). D) When quantifying the total Mfn2 protein, there was a recovery of much of the protein when the RGCs were allowed to recovery. Significantly, the recovery was in the phosphorylated isoform of Mfn2 (dark portion of bar).

Part IV: Conclusion

This thesis addresses gaps in our knowledge regarding both mitochondrial dynamics in neurodegenerative diseases, as well as its specific role with regard to the interplay of risk factors in glaucomatous disease progression. These new data support 1) the position that mitochondrial mutations do not play a role in altered mitochondrial behavior and health in the strictures of glaucoma; 2) increased expression of Mfn2 in RGCs occurs, but appears to be resultant of the degeneration of the RGC axons and transport disruption rather than causative of these effects; 3) a shift in phosphorylation state occurs in disease, contributing to the dysfunction of the mitochondria; and, 4) RGCs *in vitro* suffer degenerative changes upon exposure to pressure levels which mimic high IOP, but some level of recovery is possible when intervention occurs early. With the development of this new nanoimmunoassay targeting the mitofusins, we can clearly reflect the functional impact on mitochondria in RGCs and other tissues relevant in glaucoma, as well as other neuronal tissues.

However, we are left with a number of lingering questions regarding exactly how these changes occur and what the role of these changes are in the development or furtherance of neurodegenerative disease. Some current research in glaucoma employs a microbead assay to induce an acute variant of the disease (Sappington RM, 2006) and measure a range of outcomes, including functional changes (Chen et al., 2011), glial response (Lupien, et al., unpublished), (Dai et al., 2012), and morphological changes in RGCs (Della Santina et al., 2013). Neither this method nor other acute models (Gross et al., 2003) have been used to evaluate mitochondrial protein changes. This acute version could be quite useful for studying early changes in the mitochondrial fusion proteins based on our observation of this phenomenon.

While there are some studies available which look at the effect of knocking down mitofusin expression in cells (Misko et al., 2010), it is important to translate that work into animal models. Using the well-characterized glaucoma mouse model, where mitochondrial function is known to be compromised, we can introduce viral constructs carrying either Mfn1 or Mfn2 vectors into the eye chamber, targeting RGCs (Guy et al., 1999; Knoferle et al., 2010). Others have found the overexpression of other mitochondria-related proteins to be protective (Munemasa et al., 2010). By overexpressing the mitofusin proteins, we may see a similar protective effect, which will reflect their role in neuronal health, as well as determine whether rescue of the uncompromised phenotype is possible.

A silencing RNA construct injected into the eye will also allow for the study of mitofusins *in vivo*, and determine whether a lack of Mfn2 in RGCs is sufficient to produce a glaucomatous response. Both of these viral injection methods can be combined with the microbead model (discussed previously) to determine whether a lack of mitofusins is causative of or responsive to disease; using the microbead model with overexpression of Mfn1 or Mfn2 will allow us to examine how critical a role they may play in rescuing the degenerative process.

The data in this body of work indicate that phosphorylation is dynamically regulated by pressure, which effect may occur in a matter of hours or days. Sustained increased pressure contributes to disease progression and cell death. Further research is needed to determine how the dynamic regulation of Mfn2 phosphorylation occurs *in vivo* and if this correlates with axonal transport and energy production.

It is known that IOP causes stress on the ganglion cells in the retina and that Mfn2 becomes dephosphorylated. The dephosphorylation of Mfn2 may be tied to kinase activity. Protein phosphorylation is the most common and important form of reversible protein post-translational modification, with up to 30% of all proteins being phosphorylated at any given time (Manning et al., 2002). It plays a crucial role in biological functions and controls nearly every cellular process, including metabolism, cytoskeletal rearrangement, protein-protein interactions, protein stability, cell movement, and apoptosis. These processes depend on the highly regulated actions of kinases, through changes in the phosphorylation of key proteins, such as Mfn2. The early, but reversible, effect of pressure may be induced by the suppression of kinases active in the cell.

Kinases and phosphatases

Kinases are enzymes that modify other proteins by catalyzing the transfer of a phosphate group from ATP to target proteins. This phosphorylation usually results in a functional change of the target protein by changing activity or association with other proteins. Because kinases have such profound effects on cells, their activity must be highly regulated (Besant PG, 2003). Kinases are turned on or off by phosphorylation, sometimes by the kinase itself (i.e., autophosphorylation), by the binding of activator proteins or inhibitor proteins, or by controlling various chemical activities (Dhanasekaran and Premkumar Reddy, 1998).

Most kinases act on serine and threonine (Barford, 1996); Mfn2 has several serine and threonine modification sites. Activity of serine/threonine kinases can be regulated by specific events (e.g., DNA damage), as well as numerous chemical signals, including the actions of Ca^{2+}/calmodulin (Mumby MC, 1993). Two major factors influence activity of kinases: a) signals that activate transmembrane receptors and their associated proteins, and b) signals that inactivate the phosphatases that restrict a given kinase. Such signals include oxidant stress (Vlahopoulos, 2004), which is known to be present in glaucoma (Inman et al., 2013; Lambert W, 2008) and other neurodegenerative diseases (Lin and Beal, 2006; Twig et al., 2008), and may include the stress generated by elevated IOP.

Acting in direct opposition to kinases, phosphatases remove phosphate groups from proteins (Davies et al., 2012; Martin and Senior, 1980; Riley and Peters, 1981). The addition or removal of a phosphate group may activate or de-activate kinase signaling pathways or enable a protein-protein interaction to occur; therefore phosphatases are integral to many signal transduction pathways (Seger and Krebs, 1995). Phosphates are important in signal transduction because they regulate the proteins to which they are attached. To reverse the effect, the phosphate group is removed. This dephosphorylation sometimes occurs on its own, or is mediated by phosphatases (Zhang, 2002).

In the brain, phosphatases are present in different subcellular compartments in neuronal and glial cells, and contribute to different neuronal processes, including synaptic function. One of the major switches for neuronal activity is elevation of intracellular calcium. The degree of activation of the phosphatases is controlled by their individual sensitivities to calcium. In neuronal cells, phosphatases play a critical role at both pre- and post-synapses, in the cytoplasm and in the nucleus. These regulators are essential for maintaining the coordinated action of signaling cascades, which in neuronal cells include short-term (synaptic) and long-term (nuclear) signaling (Hsu et al., 2002). These functions are, in part, controlled by reversible protein phosphorylation. Dysregulation of their activity has been linked to several disorders including cognitive aging and neurodegeneration (Anderson and Kane, 1998; Anderson et al., 2004; Hsu et al., 2002; Sanhueza et al., 2007).

Using the known phosphorylation sites of Mfn2, we compiled a candidate list which includes 3 very strong kinase candidates: Protein Kinase A (PKA), Ca^{++}/calmodulin-dependent protein kinase II (CaMKII), and PTEN-induced putative kinase 1 (PINK1). PKA is one of 8

candidate kinases to act on Mfn2 (via ScanSite), and the only one of which correlates to one of the 6 phosphorylation sites identified via both AA sequencing and mass spectometry. PKA is one of the most ubiquitous kinases across all cell types. PKA is a strong candidate as one potential activator of Mfn2 phosphorylation, as PKA phosphorylates proteins with an exposed arginine-arginine-X-serine motif, which then activates or deactivates the protein. At S442 on Mfn2, we find an arginine-arginine-leucine-serine site.

A second candidate, CaMKII, is a multifunctional serine/threonine kinase that is activated in the presence of increased intracellular calcium, and acts as a calcium sensor and signal transducer (Anderson and Kane, 1998; Xiao et al., 1994). Neurons are rich in calcium pathways and mitochondria use calcium to signal to each other (Cali, 2012; Knoferle et al., 2010) and other organelles. It also autophosphorylates. It is a known prominent kinase in the CNS (Sanhueza et al., 2007). It is present in abundance at synapses, one of the locations of mitochondria and energy demand, and its responsiveness to intracellular Ca^{++} fit a model whereby calcium currents activate the kinase and lead to changes at the synapes (Rongo, 2002). Upon taking on Ca^{++} ions, the post-conformational change exposes hydrophobic surfaces which bind to BAA helices, which describe the Mfn2 tethering coils which mediate mitofusin oligomerization, and thus are available targets for CaMKII binding and activation.

PINK1 is also a serine-threonine kinase, which we know associates with mitochondria and is involved in ubiquitin recruitment, phosphorylation and dephosphorylation. It is a key player in Parkinson's, and has been shown to interact with the Miro/Milton complex. PINK1 protects against mitochondrial dysfunction during cellular stress, potentially by phosphorylating mitochondrial proteins, and is involved in the clearance of damaged mitochondria via the parkin protein which binds to depolarized mitochondria and induces mitophagy. It is necessary for PARK2 (a ubiquitin ligase) recruitment to dysfunctional mitochondria to initiate their degradation by recruiting ubiquitin to the regions that need recycling (pinched off to make a daughter cell that can then be degraded) (Poole et al., 2008; Poole et al., 2010; Weihofen et al., 2009; Whitworth and Pallanck, 2009).

Another possible activator in the kinase/phosphatase cascade is OGT (O-linked beta-N-acetylglucosamine transferase), an enzyme present in the Miro/Milton protein complex that couples metabolic status to the regulation of a wide variety of cellular signaling pathways by acting as a nutrient sensor. OGT catalyzes the transfer of proteins and phosphatases to

cytoplasmic, nuclear and mitochondrial proteins. Aberrant glycoslyation by OGT has been linked to neurodegenerative diseases. Details of how OGT recognizes and glycosylates its protein substrates are largely unknown. The Miro/Milton complex is involved in mitochondrial transport (Misko et al., 2010), and thus OGT may play an additional regulatory role in Mfn2 phosphorylation.

Proposed model of dephosphorylation

Dephosphorylation is a reversible post-translational modification that is a highly regulated process. The phosphorylation-dephosphorylation reaction occurs in every physiological process, and is a key process involved in inner cell and cell-to-cell signaling (Anderson and Kane, 1998; Rongo, 2002; Wei et al., 2004). As was demonstrated earlier, disease alone was sufficient to cause the dephosphorylation of Mfn2. In chapter 3, the removal of the pressure stressor from *in vitro* RGCs allowed for essential phosphorylation of Mfn2 to be reestablished. Thus, pressure may induce the dephosphorylation of Mfn2 via deactivation of an unknown kinase either as the sole action or in concert with an improper activation of a phosphatase.

In glaucoma, increases in IOP act as a stress trigger on the RGCs (Celardo et al., 2013; Gonzalez-Cabo and Palau, 2013; Rodriguez-Martinez et al., 2013). The following proposed model (Figure 4.1) demonstrates how pressure may induce the dephosphorylation of Mfn2 via deactivation of an unknown kinase or kinases. Briefly, the inhibition of the kinases allows Mfn2 to become dephosphorylated, which then interferes with mitochondrial transport and fusion. Further complications cascade from the dephosphorlyation, including the disruption of proper Ca^{++} signaling (contributing to axonal die-back), and prevents mitochondrial return to the soma for repair or phosphorylation.

While it is feasible that there is only one kinase-phosphatase pairing acting on Mfn2, it is more likely that one or more kinases are acting in concert to phosphorylate the protein. For example, PKA may act rapidly and early, while CaMKII acts more slowly with a longer effect. These two kinases have been shown to interact in conjunction with each other in cardiac tissue, causing both early and sustained effects, with PKA signaling in a biphasic fashion, and CaMKII signaling expressing slowly and persistently. Also, the two kinases appeared to act independently of the actions of the other, with sustained activation of PKA signaling not

activating CaMKII, and blocking PKA activity entirely does not prevent CaMKII from activation(Wang et al., 2004).

As our data reflect an early recovery effect of the RGCs upon removal of its stressor, pressure, this lends support to the possibility of more than one kinase being involved in the phosphorylation of Mfn2. In glaucoma, increasing IOP places stress on the cells, which may then act to suppress the kinases. If one considers the possibility of fast-acting and slower acting kinases being simultaneously present (Wang et al., 2004), removal of the pressure (stress) early may prevent the suppression of the slower acting kinases and a more rapid reversal of the dephosphorylated Mfn2 protein. In cardiac muscle, it was shown that PKA's biphasic nature created an early burst of activity followed by a smaller, later burst of activity, while CaMKII signaling was much more consistent and persistent (Wang et al., 2004). A similar sort of timed signaling of these two kinases could create both the suppression and restoration of Mfn2 phosphorylation.

To test this hypothesis, a series of experiments need to be conducted to shed light on which kinases are present, whether there is a timed reaction of multiple kinases to the application of pressure and its removal, and to further explore the role of using kinases or phosphatase inhibitors to rescue Mfn2 phosphorylation. It will also be interesting to note whether restoration of adequate Mfn2 phosphorylation reverses or slows disease progression.

The first series of experiments can be conducted in *in vitro* RGCs, with paired sets of samples being treated with one of several different kinases, examining different timing of application of the kinase, as well as. These can be set up several ways to be able to evaluate multiple outcomes (see Figure 4.2): one set can be treated with a kinase, then put under pressure to compare the result between pressure only and pressure with added kinase; another set can be placed under pressure, with kinase added to one half of the set upon removal from the pressure before measuring changes in Mfn2's phosphorylation state. In all the *in vitro* experiments, there needs to be control sets of cells maintained at ambient pressure for baseline determination.

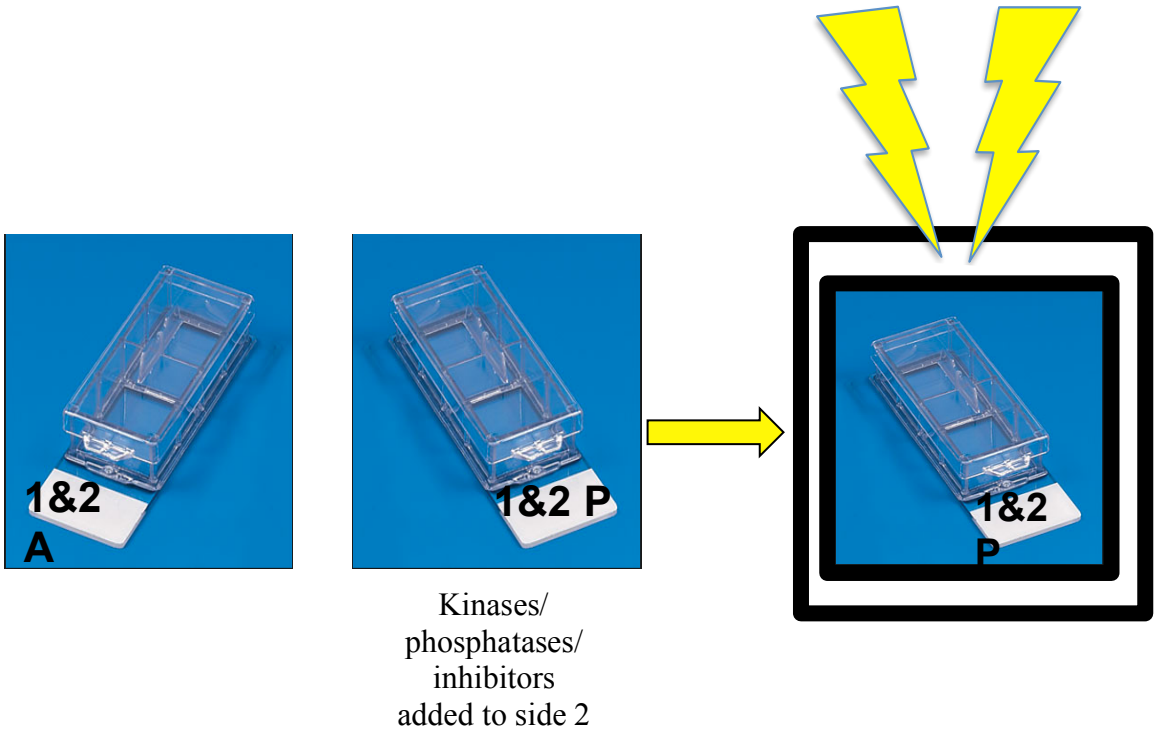

Figure 4.2 Experimental set up for RGC testing of kinases, phosphatases and inhibitors.

Results from these samples can be run on the NanoPro using the assays for Mfn2, as well as Mfn1 and ubiquitin, to quantify and compare what changes occur in protein amounts and any shift in phosphorylation state. Based on which kinases show an effect on the cells, it can be determined which kinases are active and present, and with which kinases to continue experimentation.

The next series of experiments should be conducted in *in vitro* RGCs, this time examining the effect of inhibiting kinases and stimulating phosphatases to better ascertain the role of phosphatases in the dephosphorylation of Mfn2. First, using a broad spectrum kinase inhibitor, using the same model as before (Figure 4.2), one set of RGCs is treated with the inhibitor, while the other is not. Placing both sets under pressure, and then comparing both sets with the control cells kept at ambient pressure, as well as with cells treated with inhibitors but not subjected to the stress of pressure, the varying conditions can be compared.

Again, results from these multiple conditions can be run on the NanoPro to quantify and compare what changes occur in protein amounts and any shift in phosphorylation state. The shifts in phosphorylation state will be able to confirm which action most closely mimics the

results found in the diseased tissues, and shedding light on the mechanisms involved in the decreased efficiency of Mfn2.

Running additional experiments using added phosphatases, and experiments adding phosphatase inhibitors to both cells subjected to pressure as well as cells left at ambient pressure, it can be ascertained what kind of role phosphatases play, and which specific phosphatases are acting, in the RGCs exposed to stress. By applying phosphatases to unstressed cells, it is possible that this alone can cause a response which mimics Mfn2's response in glaucoma.

A final set of *in vitro* experiments can be conducted to determine the more complex interplay of kinase inhibition and phosphatase stimulation. Through the previous experiments, which kinases and phosphatases are present and interacting in stressed RGCs can be determined. Using these specific kinases and phosphatases, the various rates at which the kinases respond to stress can be studied, allowing a further narrowing of potential targets to treat and thus mitigate the deleterious disease effects on the cells.

After it is more clearly shown which kinases and/or phosphatases are involved in the dephosphorylation of Mfn2, studies can be undertaken *in vivo* using the DBA and D2G mice. By targeting the RGCs through the injection of a lentivirus carrying an identified kinase or inhibitor, the effects of that compound can be studied in animals which naturally develop disease (DBA mice). The same effect, or the opposite effector, can also be examined in the control (D2G) animals, to verify which mechanism or mechanisms are activated in the disease process.

This additional data can lead us to a better understanding of the mechanisms behind the current pressure-lowering drugs. The data strongly suggest that the dynamic regulation of Mfn2 phosphorylation occurs during the disease process, disrupting the equilibrium of kinases and phosphatases, to the detriment of the mitochondria, and ultimately to the neurons. As adequate phosphorylation of Mfn2 correlates with normal axonal transport and energy, this future research may uncover whether pressure-lowering drugs mediate their neuroprotective effects through indirect facilitation of axonal transport and maintenance of a normal Mfn2 phosphorylation state.

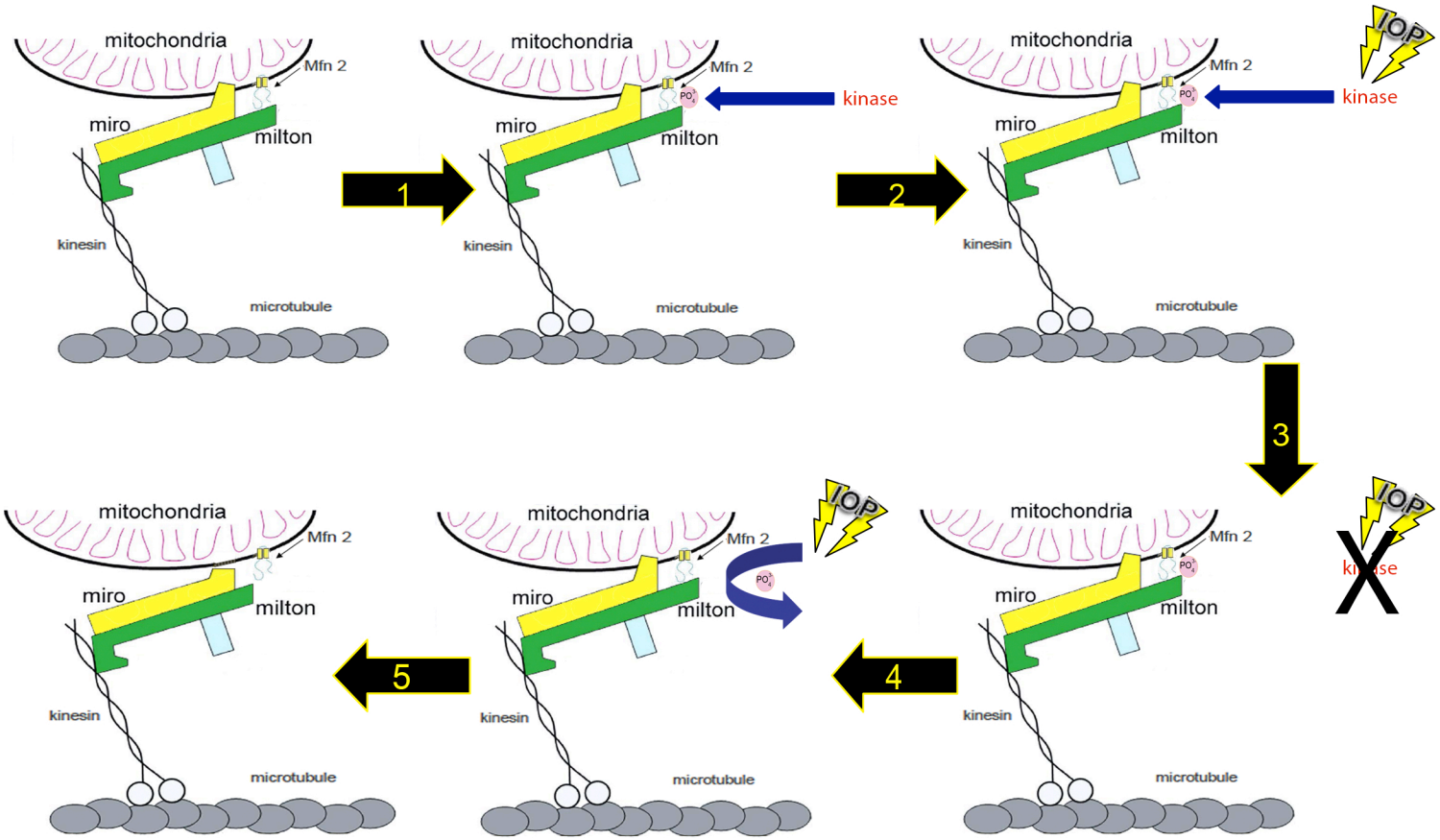

Figure 4.1 Proposed model of dephosphorylation of Mfn2
Upper left- Mfn2 is located on the outer membrane of the mitochondria, interacting with the Miro/Milton complex, and is involved in anchoring the mitochondria to the kinesin.
Upper center- Kinases active in neurons phosphorylate Mfn2, maintaining it in an active state.
Upper right- Stressors (in this model IOP) act to inhibit the kinase(s).
Lower right- Kinases are prevented from maintaining the phosphorylated state in Mfn2.
Lower center- Inhibition of the kinase(s) allows for the dephosphorylation of Mfn2 to be sustained.
Lower left- Loss of phosphorylation disrupts the anchoring of the mitochondria to the kinesin, disrupting transport. Loss of phosphorylation also interferes with normal fusion.

Part V: References

Eye diagram. UpToDate Neurology online.

Abramov, A.Y., Smulders-Srinivasan, T.K., Kirby, D.M., Acin-Perez, R., Enriquez, J.A., Lightowlers, R.N., Duchen, M.R., Turnbull, D.M., 2010. Mechanism of neurodegeneration of neurons with mitochondrial DNA mutations. Brain : a journal of neurology 133, 797-807.

Amati-Bonneau, P., Valentino, M.L., Reynier, P., Gallardo, M.E., Bornstein, B., Boissiere, A., Campos, Y., Rivera, H., de la Aleja, J.G., Carroccia, R., Iommarini, L., Labauge, P., Figarella-Branger, D., Marcorelles, P., Furby, A., Beauvais, K., Letournel, F., Liguori, R., La Morgia, C., Montagna, P., Liguori, M., Zanna, C., Rugolo, M., Cossarizza, A., Wissinger, B., Verny, C., Schwarzenbacher, R., Martin, M.A., Arenas, J., Ayuso, C., Garesse, R., Lenaers, G., Bonneau, D., Carelli, V., 2008. OPA1 mutations induce mitochondrial DNA instability and optic atrophy 'plus' phenotypes. Brain : a journal of neurology 131, 338-351.

Anderson, K.A., Kane, C.D., 1998. Ca2+/calmodulin-dependent protein kinase IV and calcium signaling. Biometals : an international journal on the role of metal ions in biology, biochemistry, and medicine 11, 331-343.

Anderson, K.A., Noeldner, P.K., Reece, K., Wadzinski, B.E., Means, A.R., 2004. Regulation and function of the calcium/calmodulin-dependent protein kinase IV/protein serine/threonine phosphatase 2A signaling complex. The Journal of biological chemistry 279, 31708-31716.

Anderson, M.G., Nair, K.S., Amonoo, L.A., Mehalow, A., Trantow, C.M., Masli, S., John, S.W., 2008. GpnmbR150X allele must be present in bone marrow derived cells to mediate DBA/2J glaucoma. BMC genetics 9, 30.

Anderson, M.G., Smith, R.S., Hawes, N.L., Zabaleta, A., Chang, B., Wiggs, J.L., John, S.W., 2002. Mutations in genes encoding melanosomal proteins cause pigmentary glaucoma in DBA/2J mice. Nature genetics 30, 81-85.

Baltan, S., Inman, D.M., Danilov, C.A., Morrison, R.S., Calkins, D.J., Horner, P.J., 2010. Metabolic vulnerability disposes retinal ganglion cell axons to dysfunction in a model of

glaucomatous degeneration. The Journal of neuroscience : the official journal of the Society for Neuroscience 30, 5644-5652.

Barford, D., 1996. Molecular mechanisms of the protein serine/threonine phosphatases. Trends Biochem. Sci. 21, 407-412.

Besant PG, T.E., Attwood PV 2003. Mammalian protein histidine kinases. Int. J. Biochem. Cell Biol. 35, 297-309.

Bielas, J.H., Loeb, L.A., 2005. Quantification of random genomic mutations. Nature methods 2, 285-290.

Bosco, A., Inman, D.M., Steele, M.R., Wu, G., Soto, I., Marsh-Armstrong, N., Hubbard, W.C., Calkins, D.J., Horner, P.J., Vetter, M.L., 2008. Reduced retina microglial activation and improved optic nerve integrity with minocycline treatment in the DBA/2J mouse model of glaucoma. Investigative ophthalmology & visual science 49, 1437-1446.

Bosco, A., Steele, M.R., Vetter, M.L., 2011. Early microglia activation in a mouse model of chronic glaucoma. J Comp Neurol 519, 599-620.

Buckingham, B.P., Inman, D.M., Lambert, W., Oglesby, E., Calkins, D.J., Steele, M.R., Vetter, M.L., Marsh-Armstrong, N., Horner, P.J., 2008. Progressive ganglion cell degeneration precedes neuronal loss in a mouse model of glaucoma. The Journal of neuroscience : the official journal of the Society for Neuroscience 28, 2735-2744.

Cali, T., Ottolini D, Brini M, 2012. Mitochondrial Ca(2+) and
neurodegeneration. Cell calcium 52, 73-85.

Calkins, D.J., 2012. Critical pathogenic events underlying progression of neurodegeneration in glaucoma. Progress in retinal and eye research 31, 702-719.

Calkins, D.J., Horner, P.J., 2012. The cell and molecular biology of glaucoma: axonopathy and the brain. Investigative ophthalmology & visual science 53, 2482-2484.

Celardo, I., Martins, L.M., Gandhi, S., 2013. Unravelling mitochondrial pathways to Parkinson's disease. Br J Pharmacol.

Chan, D.C., 2006a. Mitochondria: dynamic organelles in disease, aging, and development. Cell 125, 1241-1252.

Chan, D.C., 2006b. Mitochondrial fusion and fission in mammals. Annu Rev Cell Dev Biol 22, 79-99.

Chan, D.C., 2012. Fusion and fission: interlinked processes critical for mitochondrial health. Annual review of genetics 46, 265-287.

Chang, B., Smith, R.S., Hawes, N.L., Anderson, M.G., Zabaleta, A., Savinova, O., Roderick, T.H., Heckenlively, J.R., Davisson, M.T., John, S.W., 1999. Interacting loci cause severe iris atrophy and glaucoma in DBA/2J mice. Nature genetics 21, 405-409.

Chen, H., Detmer, S.A., Ewald, A.J., Griffin, E.E., Fraser, S.E., Chan, D.C., 2003. Mitofusins Mfn1 and Mfn2 coordinately regulate mitochondrial fusion and are essential for embryonic development. J Cell Biol 160, 189-200.

Chen, H., McCaffery, J.M., Chan, D.C., 2007. Mitochondrial fusion protects against neurodegeneration in the cerebellum. Cell 130, 548-562.

Chen, H., Vermulst, M., Wang, Y.E., Chomyn, A., Prolla, T.A., McCaffery, J.M., Chan, D.C., 2010. Mitochondrial fusion is required for mtDNA stability in skeletal muscle and tolerance of mtDNA mutations. Cell 141, 280-289.

Chen, H., Wei, X., Cho, K.S., Chen, G., Sappington, R., Calkins, D.J., Chen, D.F., 2011. Optic neuropathy due to microbead-induced elevated intraocular pressure in the mouse. Investigative ophthalmology & visual science 52, 36-44.

Chen, Y., Dorn, G.W., 2nd, 2013. PINK1-phosphorylated mitofusin 2 is a Parkin receptor for culling damaged mitochondria. Science 340, 471-475.

Chen Y, L.Y., Dorn GW 2nd, 2011. Mitochondrial fusion is essential for organelle function and cardiac homeostasis. Circ Res 109, 1327-1331.

Cho, D.H., Nakamura, T., Lipton, S.A., 2010. Mitochondrial dynamics in cell death and neurodegeneration. Cellular and molecular life sciences : CMLS 67, 3435-3447.

Chrysostomou, V., Rezania, F., Trounce, I.A., Crowston, J.G., 2013. Oxidative stress and mitochondrial dysfunction in glaucoma. Current opinion in pharmacology 13, 12-15.

Cipolat, S., Rudka, T., Hartmann, D., Costa, V., Serneels, L., Craessaerts, K., Metzger, K., Frezza, C., Annaert, W., D'Adamio, L., Derks, C., Dejaegere, T., Pellegrini, L., D'Hooge, R., Scorrano, L., De Strooper, B., 2006. Mitochondrial rhomboid PARL regulates cytochrome c release during apoptosis via OPA1-dependent cristae remodeling. Cell 126, 163-175.

Crish, S.D., Dapper, J.D., MacNamee, S.E., Balaram, P., Sidorova, T.N., Lambert, W.S., Calkins, D.J., 2013. Failure of axonal transport induces a spatially coincident increase in astrocyte BDNF prior to synapse loss in a central target. Neuroscience 229, 55-70.

Dai, C., Khaw, P.T., Yin, Z.Q., Li, D., Raisman, G., Li, Y., 2012. Structural basis of glaucoma: the fortified astrocytes of the optic nerve head are the target of raised intraocular pressure. Glia 60, 13-28.

Davies, O., Mendes, P., Smallbone, K., Malys, N., 2012. Characterisation of multiple substrate-specific (d)ITP/(d)XTPase and modelling of deaminated purine nucleotide metabolism. BMB reports 45, 259-264.

Davies, V.J., Hollins, A.J., Piechota, M.J., Yip, W., Davies, J.R., White, K.E., Nicols, P.P., Boulton, M.E., Votruba, M., 2007. Opa1 deficiency in a mouse model of autosomal dominant optic atrophy impairs mitochondrial morphology, optic nerve structure and visual function. Hum Mol Genet 16, 1307-1318.

Della Santina, L., Inman, D.M., Lupien, C.B., Horner, P.J., Wong, R.O., 2013. Differential progression of structural and functional alterations in distinct retinal ganglion cell types in a mouse model of glaucoma. The Journal of neuroscience : the official journal of the Society for Neuroscience 33, 17444-17457.

Detmer, S.A., Chan, D.C., 2007. Functions and dysfunctions of mitochondrial dynamics. Nat Rev Mol Cell Biol 8, 870-879.

Dhanasekaran, N., Premkumar Reddy, E., 1998. Signaling by dual specificity kinases. Oncogene 17, 1447-1455.

Elgass, K., Pakay, J., Ryan, M.T., Palmer, C.S., 2013. Recent advances into the understanding of mitochondrial fission. Biochimica et biophysica acta 1833, 150-161.

Eschenbacher, W.H., Song, M., Chen, Y., Bhandari, P., Zhao, P., Jowdy, C.C., Engelhard, J.T., Dorn, G.W., 2nd, 2012. Two rare human mitofusin 2 mutations alter mitochondrial dynamics and induce retinal and cardiac pathology in Drosophila. PloS one 7, e44296.

Ferrer, E., 2006. Trabecular meshwork as a new target for the treatment of glaucoma. Drug News Perspect 19, 151-158.

Flanagan, J.G., 1998. Glaucoma update: epidemiology and new approaches to medical management. Ophthalmic Physiol Opt 18, 126-132.

Frezza, C., Cipolat, S., Martins de Brito, O., Micaroni, M., Beznoussenko, G.V., Rudka, T., Bartoli, D., Polishuck, R.S., Danial, N.N., De Strooper, B., Scorrano, L., 2006. OPA1 controls apoptotic cristae remodeling independently from mitochondrial fusion. Cell 126, 177-189.

Friedman DS, W.M., Liebmann JM, Fechtner RD, Weinreb RN, 2004. An evidence-based assessment of risk factors for the progression of ocular hypertension and glaucoma. Am J Ophthalmol 138.

Frogne T, S.K., Kubicek S, Nielsen ML, Hecksher-Sørensen J, 2012. Pdx1 Is Post-Translationally Modified In vivo and Serine 61 Is the Principal Site of Phosphorylation. PloS one.

Gegg, M.E., Cooper, J.M., Chau, K.Y., Rojo, M., Schapira, A.H., Taanman, J.W., 2010. Mitofusin 1 and mitofusin 2 are ubiquitinated in a PINK1/parkin-dependent manner upon induction of mitophagy. Hum Mol Genet 19, 4861-4870.

Glater E, M.L., Stowers RS, Schwarz T, 2006. Axonal transport of mitochondrial requires milton to recruit kinesin heavy chain and is light chain independent. J Cell Biol, 545-557.

Glauser, L., Sonnay, S., Stafa, K., Moore, D.J., 2011. Parkin promotes the ubiquitination and degradation of the mitochondrial fusion factor mitofusin 1. Journal of neurochemistry 118, 636-645.

Gonzalez-Cabo, P., Palau, F., 2013. Mitochondrial pathophysiology in Friedreich's ataxia. Journal of neurochemistry 126 Suppl 1, 53-64.

Gordon, M.O., Beiser, J.A., Brandt, J.D., Heuer, D.K., Higginbotham, E.J., Johnson, C.A., Keltner, J.L., Miller, J.P., Parrish, R.K., 2nd, Wilson, M.R., Kass, M.A., 2002. The Ocular Hypertension Treatment Study: baseline factors that predict the onset of primary open-angle glaucoma. Archives of ophthalmology 120, 714-720; discussion 829-730.

Gross, R.L., Ji, J., Chang, P., Pennesi, M.E., Yang, Z., Zhang, J., Wu, S.M., 2003. A mouse model of elevated intraocular pressure: retina and optic nerve findings. Trans Am Ophthalmol Soc 101, 163-169; discussion 169-171.

Guo, X., Chen, K.H., Guo, Y., Liao, H., Tang, J., Xiao, R.P., 2007. Mitofusin 2 triggers vascular smooth muscle cell apoptosis via mitochondrial death pathway. Circ Res 101, 1113-1122.

Guy, J., Qi, X., Muzyczka, N., Hauswirth, W.W., 1999. Reporter expression persists 1 year after adeno-associated virus-mediated gene transfer to the optic nerve. Archives of ophthalmology 117, 929-937.

Howell, G.R., Libby, R.T., Jakobs, T.C., Smith, R.S., Phalan, F.C., Barter, J.W., Barbay, J.M., Marchant, J.K., Mahesh, N., Porciatti, V., Whitmore, A.V., Masland, R.H., John, S.W., 2007. Axons of retinal ganglion cells are insulted in the optic nerve early in DBA/2J glaucoma. J Cell Biol 179, 1523-1537.

Hsu, K.S., Huang, C.C., Liang, Y.C., Wu, H.M., Chen, Y.L., Lo, S.W., Ho, W.C., 2002. Alterations in the balance of protein kinase and phosphatase activities and age-related impairments of synaptic transmission and long-term potentiation. Hippocampus 12, 787-802.

Huang, P., Galloway, C.A., Yoon, Y., 2011. Control of mitochondrial morphology through differential interactions of mitochondrial fusion and fission proteins. PloS one 6, e20655.

Huang, P., Yu, T., Yoon, Y., 2007. Mitochondrial clustering induced by overexpression of the mitochondrial fusion protein Mfn2 causes mitochondrial dysfunction and cell death. European journal of cell biology 86, 289-302.

Hudson, G., Amati-Bonneau, P., Blakely, E.L., Stewart, J.D., He, L., Schaefer, A.M., Griffiths, P.G., Ahlqvist, K., Suomalainen, A., Reynier, P., McFarland, R., Turnbull, D.M., Chinnery, P.F., Taylor, R.W., 2008. Mutation of OPA1 causes dominant optic atrophy with external ophthalmoplegia, ataxia, deafness and multiple mitochondrial DNA deletions: a novel disorder of mtDNA maintenance. Brain : a journal of neurology 131, 329-337.

Inman, D.M., Horner, P.J., 2007. Reactive nonproliferative gliosis predominates in a chronic mouse model of glaucoma. Glia 55, 942-953.

Inman, D.M., Lambert, W.S., Calkins, D.J., Horner, P.J., 2013. alpha-Lipoic acid antioxidant treatment limits glaucoma-related retinal ganglion cell death and dysfunction. PloS one 8, e65389.

Inman, D.M., Sappington, R.M., Horner, P.J., Calkins, D.J., 2006. Quantitative correlation of optic nerve pathology with ocular pressure and corneal thickness in the DBA/2 mouse model of glaucoma. Investigative ophthalmology & visual science 47, 986-996.

Jarrett, S.G., Rohrer, B., Perron, N.R., Beeson, C., Boulton, M.E., 2013. Assessment of mitochondrial damage in retinal cells and tissues using quantitative polymerase chain reaction for mitochondrial DNA damage and extracellular flux assay for mitochondrial respiration activity. Methods in molecular biology 935, 227-243.

John, S.W., Smith, R.S., Savinova, O.V., Hawes, N.L., Chang, B., Turnbull, D., Davisson, M., Roderick, T.H., Heckenlively, J.R., 1998. Essential iris atrophy, pigment dispersion, and glaucoma in DBA/2J mice. Investigative ophthalmology & visual science 39, 951-962.

Johri, A., Beal, M.F., 2012. Mitochondrial dysfunction in neurodegenerative diseases. The Journal of pharmacology and experimental therapeutics 342, 619-630.

Kerrigan-Baumrind, L.A., Quigley, H.A., Pease, M.E., Kerrigan, D.F., Mitchell, R.S., 2000. Number of ganglion cells in glaucoma eyes compared with threshold visual field tests in the same persons. Investigative ophthalmology & visual science 41, 741-748.

Kiryu-Seo, S., Ohno, N., Kidd, G.J., Komuro, H., Trapp, B.D., 2010. Demyelination increases axonal stationary mitochondrial size and the speed of axonal mitochondrial transport. The Journal of neuroscience : the official journal of the Society for Neuroscience 30, 6658-6666.

Knoferle, J., Koch, J.C., Ostendorf, T., Michel, U., Planchamp, V., Vutova, P., Tonges, L., Stadelmann, C., Bruck, W., Bahr, M., Lingor, P., 2010. Mechanisms of acute axonal degeneration in the optic nerve in vivo. Proceedings of the National Academy of Sciences of the United States of America 107, 6064-6069.

Knott, A.B., Bossy-Wetzel, E., 2008. Impairing the mitochondrial fission and fusion balance: a new mechanism of neurodegeneration. Ann N Y Acad Sci 1147, 283-292.

Knott, A.B., Perkins, G., Schwarzenbacher, R., Bossy-Wetzel, E., 2008. Mitochondrial fragmentation in neurodegeneration. Nature reviews. Neuroscience 9, 505-518.

Koshiba, T., Detmer, S.A., Kaiser, J.T., Chen, H., McCaffery, J.M., Chan, D.C., 2004. Structural basis of mitochondrial tethering by mitofusin complexes. Science 305, 858-862.

Lambert W, K.J., Steele MR, Bosco A, Wu G, Inman DM, Vetter ML, Calkins DL, and Horner PJ, 2008. Dietary Lipoic Acid Attenuates Oxidative Stress and Retinal Ganglion Cell Loss in the DBA/2J Mouse Model of Glaucoma. Invest. Ophthalmol. Vis. Sci. 49, 5498.

Lambert WS, I.D., and Horner PJ, 2006. Ceruloplasmin Expression in the DBA/2 Mouse Model of Glaucoma. Invest. Ophthalmol. Vis. Sci. 47, 1241.

Lee, S., Van Bergen, N.J., Kong, G.Y., Chrysostomou, V., Waugh, H.S., O'Neill, E.C., Crowston, J.G., Trounce, I.A., 2011. Mitochondrial dysfunction in glaucoma and emerging bioenergetic therapies. Experimental eye research 93, 204-212.

Libby, R.T., Anderson, M.G., Pang, I.H., Robinson, Z.H., Savinova, O.V., Cosma, I.M., Snow, A., Wilson, L.A., Smith, R.S., Clark, A.F., John, S.W., 2005. Inherited glaucoma in DBA/2J mice: pertinent disease features for studying the neurodegeneration. Vis Neurosci 22, 637-648.

Lin, M.T., Beal, M.F., 2006. Mitochondrial dysfunction and oxidative stress in neurodegenerative diseases. Nature 443, 787-795.

Manning, G., Whyte, D.B., Martinez, R., Hunter, T., Sudarsanam, S., 2002. The protein kinase complement of the human genome. Science 298, 1912-1934.

Martin, S.S., Senior, A.E., 1980. Membrane adenosine triphosphatase activities in rat pancreas. Biochimica et biophysica acta 602, 401-418.

McBride H, N.M., Wasiak S, 2006. Mitochondria: more than just a powerhouse. Curr Biol 16, 551-560.

McKinnon, S.J., Schlamp, C.L., Nickells, R.W., 2009. Mouse models of retinal ganglion cell death and glaucoma. Experimental eye research 88, 816-824.

Misko, A., Jiang, S., Wegorzewska, I., Milbrandt, J., Baloh, R.H., 2010. Mitofusin 2 is necessary for transport of axonal mitochondria and interacts with the Miro/Milton complex. The Journal of neuroscience : the official journal of the Society for Neuroscience 30, 4232-4240.

Morrison, J.C., 2005. Elevated intraocular pressure and optic nerve injury models in the rat. J Glaucoma 14, 315-317.

Morrison, J.C., Moore, C.G., Deppmeier, L.M., Gold, B.G., Meshul, C.K., Johnson, E.C., 1997. A rat model of chronic pressure-induced optic nerve damage. Experimental eye research 64, 85-96.

Mozdy AD, S.J., 2003. A fuzzy mitochondrial fusion apparatus comes into focus. Nat Rev Mol Cell Biol 4, 468-478.

Mumby MC, W.G., 1993. Protein serine/threonine phosphatases: structure, regulation, and functions in cell growth. Physiol. Rev. 73, 673-699.

Munemasa, Y., Kitaoka, Y., Kuribayashi, J., Ueno, S., 2010. Modulation of mitochondria in the axon and soma of retinal ganglion cells in a rat glaucoma model. Journal of neurochemistry 115, 1508-1519.

Nguyen, D., Alavi, M.V., Kim, K.Y., Kang, T., Scott, R.T., Noh, Y.H., Lindsey, J.D., Wissinger, B., Ellisman, M.H., Weinreb, R.N., Perkins, G.A., Ju, W.K., 2011. A new vicious cycle involving glutamate excitotoxicity, oxidative stress and mitochondrial dynamics. Cell death & disease 2, e240.

O'Neill, R.A., Bhamidipati, A., Bi, X., Deb-Basu, D., Cahill, L., Ferrante, J., Gentalen, E., Glazer, M., Gossett, J., Hacker, K., Kirby, C., Knittle, J., Loder, R., Mastroieni, C., Maclaren, M., Mills, T., Nguyen, U., Parker, N., Rice, A., Roach, D., Suich, D., Voehringer, D., Voss, K., Yang, J., Yang, T., Vander Horn, P.B., 2006. Isoelectric focusing technology quantifies protein signaling in 25 cells. Proceedings of the National Academy of Sciences of the United States of America 103, 16153-16158.

Poole, A.C., Thomas, R.E., Andrews, L.A., McBride, H.M., Whitworth, A.J., Pallanck, L.J., 2008. The PINK1/Parkin pathway regulates mitochondrial morphology. Proceedings of the National Academy of Sciences of the United States of America 105, 1638-1643.

Poole, A.C., Thomas, R.E., Yu, S., Vincow, E.S., Pallanck, L., 2010. The mitochondrial fusion-promoting factor mitofusin is a substrate of the PINK1/parkin pathway. PloS one 5, e10054.

Rangarajan, K.V., Lawhn-Heath, C., Feng, L., Kim, T.S., Cang, J., Liu, X., 2011. Detection of visual deficits in aging DBA/2J mice by two behavioral assays. Current eye research 36, 481-491.

Riley, M.V., Peters, M.I., 1981. The localization of the anion-sensitive ATPase activity in corneal endothelium. Biochimica et biophysica acta 644, 251-256.

Rodriguez-Martinez, E., Martinez, F., Espinosa-Garcia, M.T., Maldonado, P., Rivas-Arancibia, S., 2013. Mitochondrial dysfunction in the hippocampus of rats caused by chronic oxidative stress. Neuroscience 252, 384-395.

Rongo, C., 2002. A fresh look at the role of CaMKII in hippocampal synaptic plasticity and memory. BioEssays : news and reviews in molecular, cellular and developmental biology 24, 223-233.

Sanhueza, M., McIntyre, C.C., Lisman, J.E., 2007. Reversal of synaptic memory by Ca2+/calmodulin-dependent protein kinase II inhibitor. The Journal of neuroscience : the official journal of the Society for Neuroscience 27, 5190-5199.

Santel, A., Fuller, M.T., 2001. Control of mitochondrial morphology by a human mitofusin. Journal of cell science 114, 867-874.

Sappington RM, C.D., 2006. The microbead occlusion model: a paradigm for induced ocular hypertension in rats and mice. Invest. Ophthalmol. Vis. Sci. 47, 3860-3869.

Sappington, R.M., Chan, M., Calkins, D.J., 2006. Interleukin-6 protects retinal ganglion cells from pressure-induced death. Investigative ophthalmology & visual science 47, 2932-2942.

Seger, R., Krebs, E.G., 1995. The MAPK signaling cascade. FASEB journal : official publication of the Federation of American Societies for Experimental Biology 9, 726-735.

Song, Z., Ghochani, M., McCaffery, J.M., Frey, T.G., Chan, D.C., 2009. Mitofusins and OPA1 mediate sequential steps in mitochondrial membrane fusion. Mol Biol Cell 20, 3525-3532.

Soto, I., Oglesby, E., Buckingham, B.P., Son, J.L., Roberson, E.D., Steele, M.R., Inman, D.M., Vetter, M.L., Horner, P.J., Marsh-Armstrong, N., 2008. Retinal ganglion cells downregulate gene expression and lose their axons within the optic nerve head in a mouse glaucoma model. The Journal of neuroscience : the official journal of the Society for Neuroscience 28, 548-561.

Tanaka, A., Cleland, M.M., Xu, S., Narendra, D.P., Suen, D.F., Karbowski, M., Youle, R.J., 2010. Proteasome and p97 mediate mitophagy and degradation of mitofusins induced by Parkin. J Cell Biol 191, 1367-1380.

Tanwar, M., Dada, T., Sihota, R., Dada, R., 2010. Mitochondrial DNA analysis in primary congenital glaucoma. Molecular vision 16, 518-533.

Twig, G., Elorza, A., Molina, A.J., Mohamed, H., Wikstrom, J.D., Walzer, G., Stiles, L., Haigh, S.E., Katz, S., Las, G., Alroy, J., Wu, M., Py, B.F., Yuan, J., Deeney, J.T., Corkey, B.E., Shirihai, O.S., 2008. Fission and selective fusion govern mitochondrial segregation and elimination by autophagy. EMBO J 27, 433-446.

Uo, T., Dworzak, J., Kinoshita, C., Inman, D.M., Kinoshita, Y., Horner, P.J., Morrison, R.S., 2009. Drp1 levels constitutively regulate mitochondrial dynamics and cell survival in cortical neurons. Experimental neurology 218, 274-285.

Vermulst, M., Bielas, J.H., Kujoth, G.C., Ladiges, W.C., Rabinovitch, P.S., Prolla, T.A., Loeb, L.A., 2007. Mitochondrial point mutations do not limit the natural lifespan of mice. Nature genetics 39, 540-543.

Vermulst, M., Bielas, J.H., Loeb, L.A., 2008. Quantification of random mutations in the mitochondrial genome. Methods 46, 263-268.

Vlahopoulos, S., Zoumpourlis, VC 2004. JNK: a key modulator of intracellular signaling. Biochemistry 69, 844-854.

Wang, W., Zhu, W., Wang, S., Yang, D., Crow, M.T., Xiao, R.P., Cheng, H., 2004. Sustained beta1-adrenergic stimulation modulates cardiac contractility by Ca2+/calmodulin kinase signaling pathway. Circ Res 95, 798-806.

Wei, J., Zhang, M., Zhu, Y., Wang, J.H., 2004. Ca(2+)-calmodulin signalling pathway up-regulates GABA synaptic transmission through cytoskeleton-mediated mechanisms. Neuroscience 127, 637-647.

Weihofen, A., Thomas, K.J., Ostaszewski, B.L., Cookson, M.R., Selkoe, D.J., 2009. Pink1 forms a multiprotein complex with Miro and Milton, linking Pink1 function to mitochondrial trafficking. Biochemistry 48, 2045-2052.

Whitmore, A.V., Libby, R.T., John, S.W., 2005. Glaucoma: thinking in new ways-a role for autonomous axonal self-destruction and other compartmentalised processes? Progress in retinal and eye research 24, 639-662.

Whitworth, A.J., Pallanck, L.J., 2009. The PINK1/Parkin pathway: a mitochondrial quality control system? Journal of bioenergetics and biomembranes 41, 499-503.

Xiao, R.P., Cheng, H., Lederer, W.J., Suzuki, T., Lakatta, E.G., 1994. Dual regulation of Ca2+/calmodulin-dependent kinase II activity by membrane voltage and by calcium influx. Proceedings of the National Academy of Sciences of the United States of America 91, 9659-9663.

Youle, R.J., van der Bliek, A.M., 2012. Mitochondrial fission, fusion, and stress. Science 337, 1062-1065.

Yu-Wai-Man, P., Griffiths, P.G., Burke, A., Sellar, P.W., Clarke, M.P., Gnanaraj, L., Ah-Kine, D., Hudson, G., Czermin, B., Taylor, R.W., Horvath, R., Chinnery, P.F., 2010a. The prevalence and natural history of dominant optic atrophy due to OPA1 mutations. Ophthalmology 117, 1538-1546, 1546 e1531.

Yu-Wai-Man, P., Griffiths, P.G., Gorman, G.S., Lourenco, C.M., Wright, A.F., Auer-Grumbach, M., Toscano, A., Musumeci, O., Valentino, M.L., Caporali, L., Lamperti, C., Tallaksen, C.M., Duffey, P., Miller, J., Whittaker, R.G., Baker, M.R., Jackson, M.J., Clarke, M.P., Dhillon, B., Czermin, B., Stewart, J.D., Hudson, G., Reynier, P., Bonneau, D., Marques, W., Jr., Lenaers, G., McFarland, R., Taylor, R.W., Turnbull, D.M., Votruba, M., Zeviani, M., Carelli, V., Bindoff, L.A., Horvath, R., Amati-Bonneau, P., Chinnery, P.F., 2010b. Multi-system neurological disease is common in patients with OPA1 mutations. Brain : a journal of neurology 133, 771-786.

Yu-Wai-Man, P., Trenell, M.I., Hollingsworth, K.G., Griffiths, P.G., Chinnery, P.F., 2011. OPA1 mutations impair mitochondrial function in both pure and complicated dominant optic atrophy. Brain : a journal of neurology 134, e164.

Zhang, Z., 2002. Protein tyrosine phosphatases: structure and function, substrate specificity, and inhibitor development. Annu. Rev. Pharmacol. Toxicol. 42, 209-234.

Zuchner, S., Mersiyanova, I.V., Muglia, M., Bissar-Tadmouri, N., Rochelle, J., Dadali, E.L., Zappia, M., Nelis, E., Patitucci, A., Senderek, J., Parman, Y., Evgrafov, O., Jonghe, P.D., Takahashi, Y., Tsuji, S., Pericak-Vance, M.A., Quattrone, A., Battaloglu, E., Polyakov, A.V.,

Timmerman, V., Schroder, J.M., Vance, J.M., 2004. Mutations in the mitochondrial GTPase mitofusin 2 cause Charcot-Marie-Tooth neuropathy type 2A. Nature genetics 36, 449-451.